



**Atomic Layer Deposition in Nanostructured Photovoltaics:
Tuning Optical, Surface and Electronic Properties**

Journal:	<i>Nanoscale</i>
Manuscript ID:	NR-FEA-04-2015-002080.R1
Article Type:	Feature Article
Date Submitted by the Author:	20-May-2015
Complete List of Authors:	Palmstrom, Axel; Stanford University, Dept. of Chemical Engineering Santra, Pralay; Stanford University, Dept. of Chemical Engineering Bent, Stacey; Stanford University, Department of Chemical Engineering

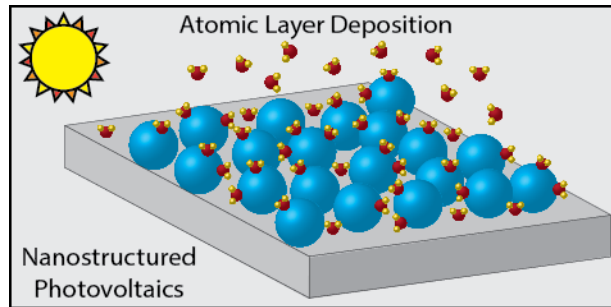
Atomic Layer Deposition in Nanostructured Photovoltaics: Tuning Optical, Electronic and Surface Properties

Axel F. Palmstrom, Pralay K. Santra and Stacey F. Bent*

Department of Chemical Engineering, Stanford University, Stanford, California
94305, United States
[E-mail: sbent@stanford.edu]

Abstract

Nanostructured materials offer key advantages for third-generation photovoltaics, such as the ability to achieve high optical absorption together with enhanced charge carrier collection using low cost components. However, the extensive interfacial areas in nanostructured photovoltaic devices can cause high recombination rates and a high density of surface electronic states. In this feature article, we provide a brief review of some nanostructured photovoltaic technologies including dye-sensitized, quantum dot sensitized and colloidal quantum dot solar cells. We then introduce the technique of atomic layer deposition (ALD), which is a vapor phase deposition method using a sequence of self-limiting, surface reaction steps to grow thin, uniform and conformal films. We discuss how ALD has established itself as a promising tool for addressing different aspects of nanostructured photovoltaics. Examples include the use of ALD to synthesize absorber materials for both quantum dot and plasmonic solar cells, to grow barrier layers for dye and quantum dot sensitized solar cells, and to infiltrate coatings into colloidal quantum dot solar cell to improve charge carrier mobilities as well as stability. We also provide an example of monolayer surface modification in which adsorbed ligand molecules on quantum dots are used to tune the band structure of colloidal quantum dot solar cells for improved charge collection. Finally, we comment on the present challenges and future outlook of the use of ALD for nanostructured photovoltaics.

Table of Contents Image:

This review highlights applications of atomic layer deposition for third generation photovoltaics, including light absorption, barrier layer formation and passivation.



Axel F. Palmstrom

Axel F. Palmstrom is from Edina, Minnesota. He received a B.S. degree in Chemical Engineering from the University of California, Santa Barbara in 2012. Axel is currently a PhD candidate in the Department of Chemical Engineering at Stanford University. His research interests include surface and interface engineering for energy applications, including photovoltaics and batteries. Axel's current research focuses on ALD for inorganic functionalization of colloidal quantum dot solar cells.



Pralay K. Santra

Pralay K. Santra is currently a postdoctoral fellow in Prof. Stacey F. Bent's research group, Department of Chemical Engineering at Stanford University. He did his M.S. and Ph.D. from Indian Institute of Science, Bangalore. Prior to joining Bent group, Pralay spent first two years of his postdoctoral research at University of Notre Dame, Indiana. His research interests include understanding optical and electronic properties of quantum dots and their applications in photovoltaics.



Stacey F. Bent

Stacey F. Bent is the Jagdeep and Roshni Singh Professor in the School of Engineering at Stanford University, where she also Professor of Chemical Engineering and Professor, by courtesy, of Chemistry, Electrical Engineering, and Materials Science and Engineering. She earned her B.S. degree from U.C. Berkeley and her Ph.D. degree from Stanford. After carrying out postdoctoral studies at Bell Laboratories and serving as Assistant Professor at New York University, she joined Stanford in 1998. Her research emphasizes fundamental surface and materials chemistry with applications in nanoelectronics and sustainable energy, including solar cells, solar fuels, and catalysts. She is Director of the TomKat Center for Sustainable Energy and is Associate Editor of Chemistry of Materials.

1. Introduction

1.1 Third Generation Photovoltaics

Global power consumption is currently 17 TW, but is expected to increase to 35 TW by 2050. Of this 17 TW, 80 % comes from fossil fuels in the form of oil, coal, and natural gas.¹ These sources of energy are non-sustainable and have significant environmental impacts resulting, for example, from CO₂ emissions that affect climate change and other types of pollution. It is necessary to transition towards renewable and environmentally-friendly energy sources as the global energy demand grows.

Solar energy is the most abundant renewable energy resource. An estimated 120,000 TW of solar power hits the earth and, of this, 600 TW is practical to collect.² Despite the abundance of solar energy, direct solar technologies only account for 1.1 % of the 2012 energy supply.¹ This is due to the economics and non-continuous power generation of solar technology. Although solar cost is decreasing and grid parity has now been achieved with crystalline solar cells in many countries,³ widespread adoption of solar has not yet occurred. In order to increase solar power generation, the cost per Watt must be further decreased. Module cost is less than half of the cost of solar installation, with other factors such as shipping, labor, permits, and inspection making up the majority of the cost.^{4,5} Because the balance of system costs scale with the size of the installation, more efficient cells which require less area per module can reduce overall costs. This drives the development of low-cost, high-efficiency solar cells, known as “third generation” photovoltaics (PV). Developing a diversity of third generation PV technologies will help address a broad range of applications.

Third generation PV technologies, by definition, must have theoretical efficiencies above the Shockley-Queisser limit at costs of \$0.20/W.⁶⁻⁸ There are several ways to break the Shockley-Queisser limit, including multi-junction devices, hot carrier injection and carrier multiplication (or multiple exciton generation).^{9, 10} The low cost condition of next generation photovoltaics favors the use of thin film technologies without high purity materials requirements and inexpensive fabrication.

1.2 Why Nanostructured Photovoltaics?

Silicon solar cells require low defect density for high efficiency. Minority carrier lifetimes of ~20 μ s are needed for efficient carrier collection and are only achievable with defect and impurity levels below $\sim 10^{-3}$ parts per million (ppm).¹¹ Achieving solar grade silicon is expensive, and processed silicon is projected to account for over 40 % of the total module costs in 2020 despite high silicon abundance.¹² Second generation technologies, such as copper indium gallium selenide (CIGS) and cadmium telluride (CdTe), focused on reducing materials cost with thin film absorbers.¹³ Third generation PV is looking to reduce costs even further through low cost deposition methods of materials that contain earth abundant elements and do not have strict purity requirements. At the same time, theoretical efficiencies will be pushed higher through advantages associated with nanostructuring, including short transport distances, rapid charge transfer and enhanced light absorption.¹⁴

Nanostructuring offers several key benefits to help reach the goals of next generation PV devices. The low-cost materials and deposition techniques required to reach \$0.20/W tend to have higher defect density and imperfect interfaces in comparison to technologies such as single crystal silicon, leading to shorter minority carrier diffusion lengths in these films. As a consequence, generated charges must be collected within short distances in order to obtain high efficiency. For this reason, absorber thicknesses are on the order of hundreds of nanometers for most third generation PV technologies. Many semiconducting materials, however, will not approach complete light absorption with these thicknesses, and there is a tradeoff between the number of charges that can be generated and the internal quantum efficiency of the device. In order to improve this relationship, in some designs the substrate surface is textured through nanostructuring to allow higher absorber loading without increasing absorber film thickness, thereby improving light absorption while maintaining short transport distances.^{15, 16} When the diffusion distance is very short, as in the case of a dye molecule or quantum dot directly on a surface such as TiO₂, electron injection occurs on the femtosecond time scale.^{17, 18} These types of devices have the potential to utilize hot carrier injection, multiple exciton generation, and multiband and impurity level phenomena to break the Shockley-Queisser limit.

Despite the advantages of nanostructured, third generation PV, current efficiencies in such devices remain lower than those of second generation thin film devices. Low realized efficiencies are often tied to the drawback of high surface area, i.e. higher total area for recombination and a high density of surface electronic states. Although the performance-limiting parameter will depend on the device architecture and materials chosen, one way to mitigate such effects is to passivate or otherwise modify the interfaces of the nanostructured systems. In this feature article, we will describe some of the methods that have used to engineer interfaces in nanostructured PV, focusing primarily on the technique of atomic layer deposition (ALD). We will first provide a brief review of some third generation PV technologies including dye-sensitized, quantum dot sensitized and colloidal quantum dot solar cells. We will then introduce ALD and discuss how ALD and relevant non-ALD surface modification has been used to address challenges in these next generation PV technologies.

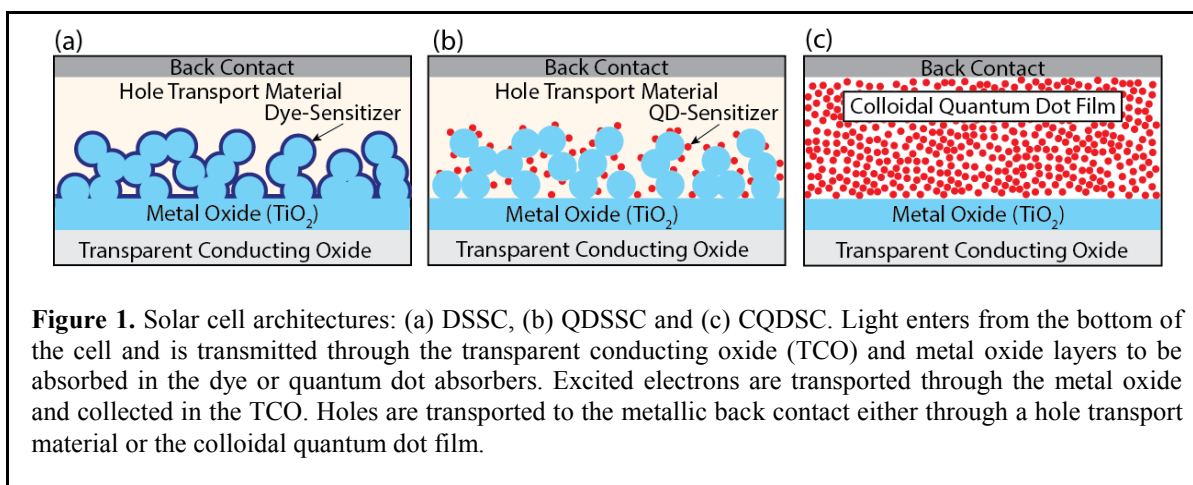
1.3 Solar Technologies Discussed in This Review

1.3.1 Dye-sensitized solar cell

The dye-sensitized solar cell (DSSC)^{19, 20} consists of a monolayer of absorber dye molecules deposited on a mesoporous wide-band-gap metal oxide, often TiO₂, created from a nanoparticle paste as shown schematically in Figure 1a. The pores of the wide-band-gap oxide are filled with a hole transport material (HTM), either a liquid redox electrolyte or a solid-state hole conducting material, designed to regenerate dye molecules after injection of an electron into the metal oxide. This design was first introduced by O'Regan and Grätzel in 1991 and differs from conventional p-n junction solar cells in a few critical ways: the charge generation and charge transport occur in separate materials, a high surface area substrate is used, and devices function without the strict purity requirements of most thin film solar technologies.²¹ Recent advances in

DSSCs have pushed efficiencies as high as 13 % using engineered donor- π -acceptor dyes with an I/I_3^- electrolyte.²² A challenge with DSSCs is the tradeoff that occurs with the thickness of the metal oxide layer: increased light absorption achieved with a thicker dye-coated film of mesoporous metal oxide competes with faster recombination rates and slower charge transport as a result of the increased surface area and incomplete infilling as the metal oxide layer gets thicker.

Liquid electrolyte and solid-state HTMs represent two different classes of DSSCs. The highest efficiency devices are made with liquid I/I_3^- redox couple electrolytes that offer deep pore penetration, long electron lifetimes and high mobilities,²³ leading to low recombination rates and long electron diffusion lengths.²⁴ Some drawbacks to liquid electrolytes, however, include a complex redox chemistry,²⁵ corrosion of metal contacts, flammability, poor stability and leakage.^{24, 26-28} Solid-state electrolytes can circumvent these limitations and are therefore desirable from the standpoint of stability and practical cell design. Excluding perovskite solar cells, which in some instances are considered solid-state DSSCs, the record efficiency for solid-state DSSCs is 8.51 %.²⁹ One approach that has received much attention for increasing the efficiency of DSSCs is to reduce recombination at the metal oxide/dye/HTM interface through the application of a barrier layer. ALD has proven to be a powerful method for depositing the barrier layer because it allows for conformal coating of the mesoporous metal oxide and precise tuning of the barrier layer thickness.



1.3.2 Quantum dot sensitized solar cell

Quantum dot solar cells absorb light in quantum-confined nanoparticles, resulting in a size-dependent absorption spectrum and allowing for modulation of the absorber's valence and conduction bands. Quantum dot sensitized solar cells (QDSSCs) take advantage of the developed low-cost, high-surface area mesoporous metal oxide architecture used in DSSCs.³⁰ QDSSCs, as the name suggests, employ quantum dots as the sensitizer (absorber) in place of DSSC dye molecules (Figure 1b). The quantum dots are deposited by several methods including chemical bath deposition,^{31, 32} electrodeposition³³ and successive ionic layer absorption and reaction.³⁴ One challenge for QDSSCs, however, is that the quantum dot surface coverage is low compared to that

of a dye and has been measured to be approximately 14 % in some cases.³⁵ Solar absorption could be improved for a given device thickness if a higher quantum dot loading could be achieved. Furthermore, low QD coverage can result in a direct metal oxide/HTM interface that can lead to surface recombination. The interface recombination problem is compounded by the inability to use the I/I_3^- redox couple electrolyte due to corrosion of semiconducting quantum dot materials.³⁶ QDSSC devices have been reported to have efficiencies as high as 7.04 %.³⁷ As with DSSCs, there is the potential to improve the efficiency through the use of barrier layers grown by ALD. In addition, recent work has explored an alternative method of forming the QDs via gas-phase ALD.

1.3.3 Colloidal quantum dot solar cell

Colloidal quantum dot (CQD) photovoltaics³⁸ have recently received significant interest due to the size tunable band gap, solution processable fabrication, potential for multiple exciton generation, and the rapid improvement in photovoltaic efficiency over the past few years, with a record reported device efficiency of 9.2 %.³⁹ Lead chalcogenides (PbS and PbSe) are the most studied materials in this field because of multiple exciton generation, ideal range of tunable bandgap, and facile charge transport via hopping mechanisms.^{40, 41} The facile charge transport arises from a large Bohr-exciton radius, high density of states and a large dielectric constant, resulting in strong QD-QD coupling of lead chalcogenide films.⁴²

In a typical colloidal quantum dot solar cell (Figure 1c), quantum dots serve as the *p*-type material and the metal oxide is used as the *n*-type material. The QD layer is depleted near the interface due to the *p-n* junction.⁴³ The excitons generated within this depleted QD layer split, and the resulting electrons and holes are transported to the metal oxide and back contact, respectively. Harvesting of these charge carriers strongly depends on the electric field of the depletion region in CQD solar cells. Earlier reports^{38, 44} have shown that commonly used PbSe and PbS based CQD solar cells remain fully depleted (hence called depleted heterojunction quantum dot solar cells) at the short circuit condition. However, the operating point of interest of a solar cell is at its maximum power point (MPP), which is achieved at forward bias. The depletion width region decreases under forward bias, and collection of charge carriers outside the depletion region solely depends on diffusion. Solar cells from quantum dots passivated with small chain bidentate organic molecules (e.g., 3-mercaptopropionic acid, MPA) have low mobilities ($10^{-3} - 10^{-2} \text{ cm}^2\text{V}^{-1}\text{s}^{-1}$), which prevents efficient collection of charge carriers outside the depletion region before recombination. To improve the photovoltaic performance of CQD solar cells, one either needs to improve the diffusion length and charge carrier mobilities or extend the depletion region within the CQD film operating at the MPP. Recent studies have shown that CQD cells can benefit from inorganic infilling of the colloidal film for more complete QD passivation and increased film stability.⁴² ALD, which provides an excellent method for infilling porous structures, has been investigated for this application. In addition, other surface functionalization strategies, such as ligand exchange, can significantly affect the electronic properties of the QDs and hence can be used to tune the electronic band structure of the CQD cells.

2. Introduction to Atomic Layer Deposition

Atomic layer deposition (ALD) was originally referred to as “atomic layer epitaxy” and was first developed for ZnS growth in the 1970s by Suntola and Antson.^{45,46} ALD is a self-limiting, vapor-phase deposition technique that occurs through sequential surface reactions. An ALD precursor cannot react with itself and, as such, the self-limiting nature of ALD arises through surface saturation, which is defined as the point at which the net precursor adsorption rate approaches zero. After saturation, additional precursor exposure time will not increase the amount of precursor adsorption. The schematic in Figure 2 illustrates the ALD cycle. In the first step, a reactant is pulsed into a reaction chamber and adsorbs onto the surface of a clean substrate. After reaching saturation, excess reactant is purged with an inert gas. A counter-reactant is then introduced to the system and reacts with the original reactant adsorbed to the substrate surface. Finally, excess counter-reactant is purged from the system. This process is repeated to increase ALD film thickness. Typical growth rates are $\sim 1 \text{ \AA/cycle}$. ALD is not a line-of-site process and hence it is capable of conformally coating both planar and porous materials.

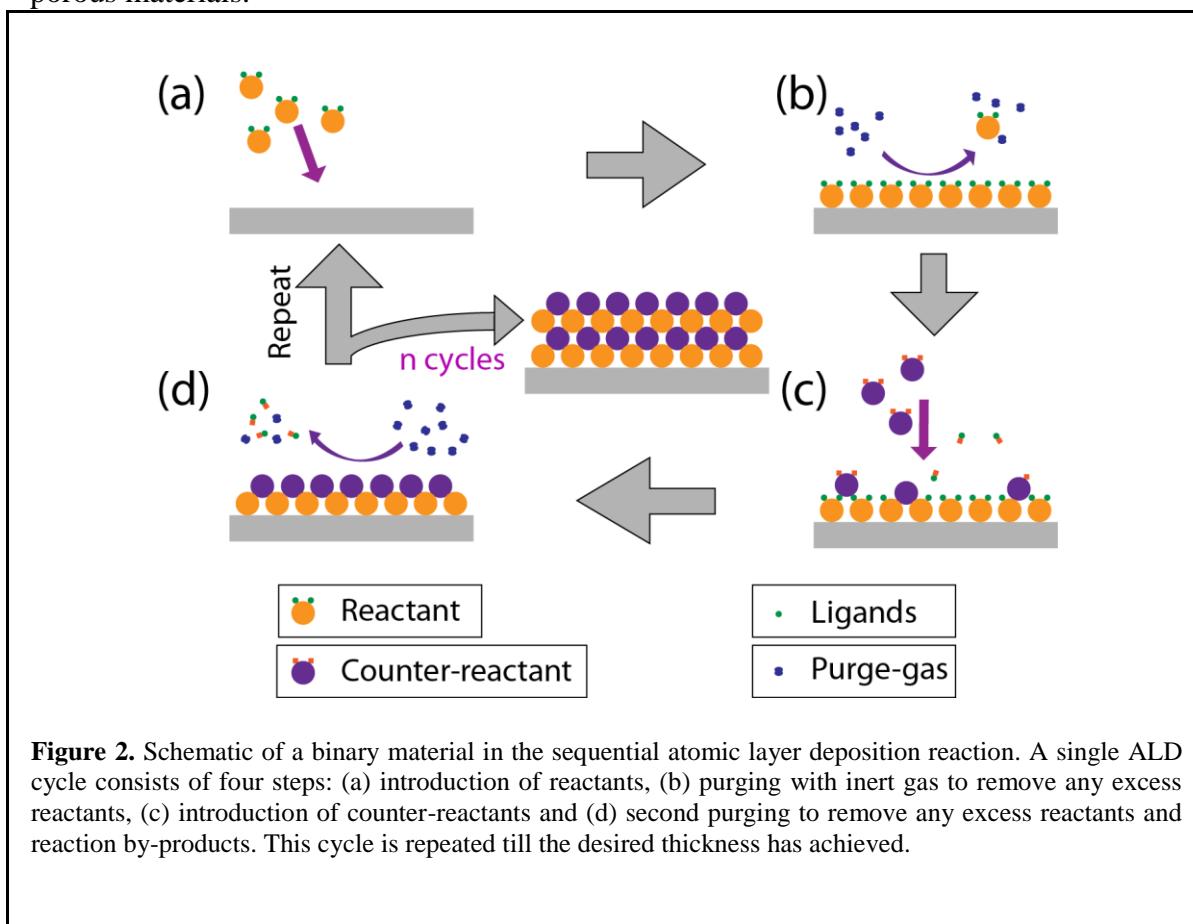


Figure 2. Schematic of a binary material in the sequential atomic layer deposition reaction. A single ALD cycle consists of four steps: (a) introduction of reactants, (b) purging with inert gas to remove any excess reactants, (c) introduction of counter-reactants and (d) second purging to remove any excess reactants and reaction by-products. This cycle is repeated till the desired thickness has achieved.

Temperature plays an important role in the ALD process. ALD typically occurs at moderately elevated temperatures to provide for enough thermal energy to drive a complete reaction between the reactant and counter-reactant. If the temperature is too

high, surface species can desorb, leading to incomplete surface coverage, or the precursors may thermally decompose on the surface. At lower temperatures, the reaction between reactant and counter-reactant may not be driven to completion or the reaction precursors may condense on the surface of the substrate, leaving more than a monolayer.⁴⁷ Precursor decomposition and condensation can result in uncontrolled CVD like growth with higher than expected per cycle growth rates while surface desorption or an incomplete reaction can result in lower than expected growth rates. This leaves an ideal temperature range known as the “ALD window” which describes the temperature range for pure ALD processes.⁴⁷⁻⁴⁹ The majority of ALD surface reactions are driven by thermal energy; however, high temperatures can be incompatible with certain substrates and less economical from a manufacturing standpoint. An alternative to thermal ALD is plasma-assisted or plasma enhanced ALD where highly reactive plasma species can reduce the thermal energy required for a surface reaction to take place and activate certain precursors that would not grow under standard thermal ALD. Profijt et al. provides a detailed review of the challenges and benefits associated with plasma-assisted ALD.⁵⁰

The initial process in ALD growth, which may last several cycles, is nucleation. Nucleation is controlled by the interaction of the precursors with the substrate and often is dependent upon substrate surface treatment as well as the type of surface sites available for growth. For example, our group has shown that nucleation of platinum ALD on highly ordered pyrolytic graphite results in nucleation on the step edges only and the formation of lateral nanowires along the step edges after subsequent deposition cycles.⁵¹ In general, it is understood that initial nucleation results in the formation of islands that enlarge according to Volmer-Weber growth and coalesce into a continuous film.⁴⁷ This process typically takes tens of ALD cycles and is known as the nucleation or incubation regime characterized by a lower than expected growth rate and film density. Nucleation is often improved by controlling the surface chemistry by processes such as ultra-violet ozone cleaning in order to remove organics and leave behind a hydroxyl terminated surface that reacts more readily with many ALD precursors resulting in a more complete reaction with the substrate surface and improved nucleation.⁵² Subsequent film growth after nucleation is dependent upon processing conditions (i.e. precursor choice, temperature, substrate etc.). One growth characteristic is film crystallinity. Miikkulainen et al. has analyzed a variety of ALD systems to highlight trends in how process parameters can affect film crystallinity.⁵³

Precursor choice is an important consideration, especially when ALD is to be applied to sensitive nanostructured solar cells. Some properties to consider include the temperature window enabled by a given precursor, since many solar cells may not be stable at high temperatures, the diffusion properties through narrow pores, and the compatibility of not only the reactants/counter reactants (such as ozone or plasma) but also reaction byproducts, such as HCl formed from chloride precursors. Additional information on selection of ALD precursors as well as a thorough summary of developed precursors can be found for in ref.⁵³ for general ALD and in ref.⁴⁹ for ALD systems applied to solar technology.

Nanostructured photovoltaics inherently have high surface area and, as a result, their electronic properties, charge transport and performance are sensitive to effects originating from surfaces and interfaces. As a sequential, gas-phase deposition technique capable of depositing films over nanostructured surfaces with sub-angstrom control and with recent advances in high throughput spatial ALD methods,⁵⁴ ALD is ideally suited for addressing the challenges facing third generation PV technologies through surface and interface modification. In this article, we will discuss the applications of ALD in the field of nanostructured photovoltaics with an emphasis on areas relevant to our laboratory, namely absorbers, barrier layers and passivation layers. For a more complete review of the application of ALD to photovoltaics, the reader is referred to ref.^{49, 55, 56} and references therein. The use of ALD for solar cell absorbers, recombination barriers, and colloidal film infiltration will be described in the subsequent sections.

3.1. Absorbers

Atomic layer deposition offers many advantages for conformal film growth. However, it is typically not applied to the deposition of absorber materials (usually 100's of nanometers thick) because of its very slow growth rates. ALD will only be advantageous in special cases of PV where ultrathin films or small particles are to be used in the absorbers. We will discuss two such special cases where ALD has been used to form the absorber layer: plasmonic solar cells where light concentration is used to confine absorption to very thin layers, and QD sensitized cells where the absorbers are QDs deposited on high surface area substrates by ALD.

3.1.1. QD Sensitizers in QDSSCs

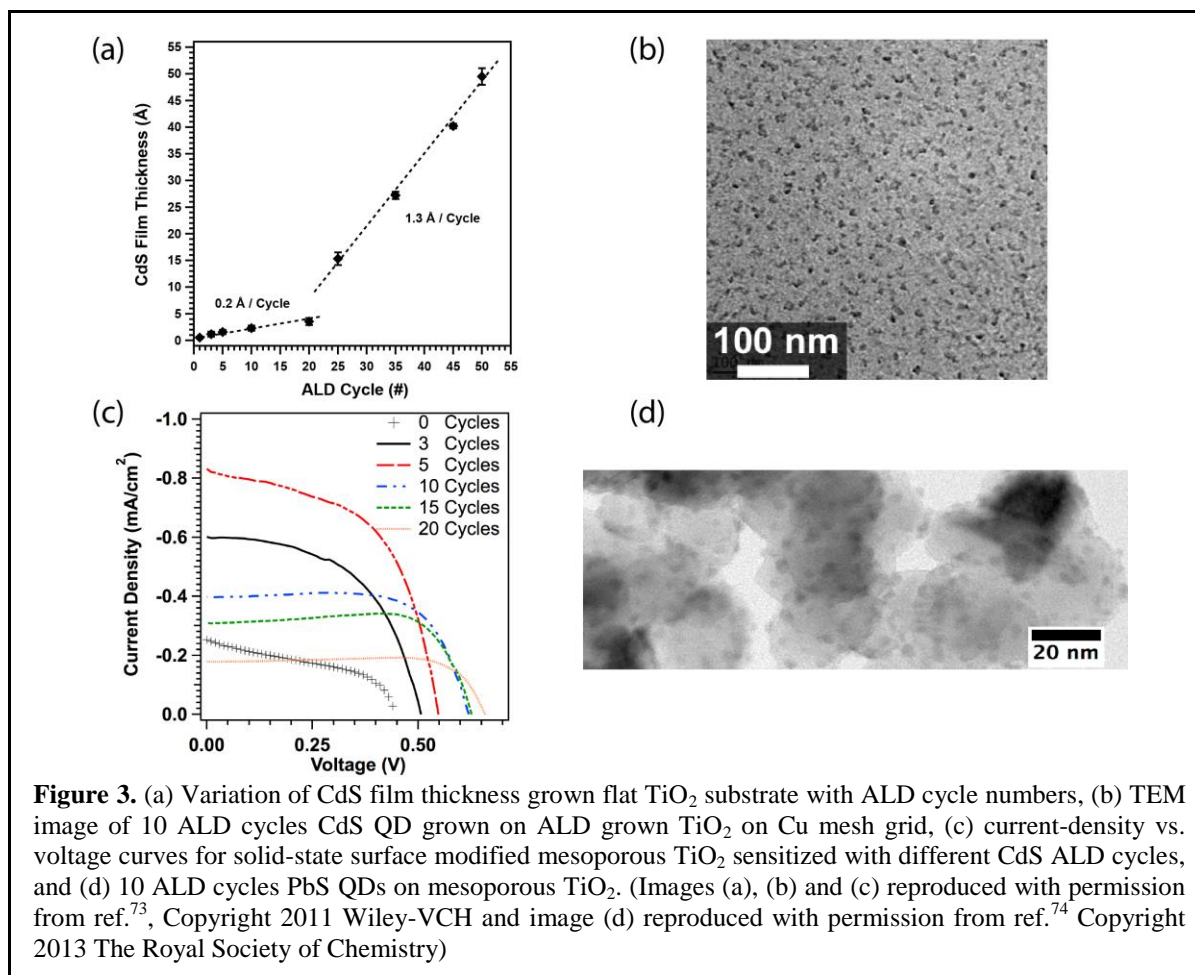
QDs have been considered for use as components in third generation PV because they possess several interesting properties, e.g., high absorption coefficients,⁵⁷ easy tunability of bandgap by size⁵⁸ or composition variation,⁵⁹ and tunable band positions through modification of their surfaces.^{60, 61} QDs have also shown the possibility of hot electron transfer⁶² and multiple exciton generation (MEG)⁶³. As described in Section 1.3, quantum dot sensitized solar cells (QDSSCs) have a similar structure to that of dye sensitized solar cells²¹ where light absorbers in QDSSCs are the quantum dots attached to the mesoporous metal oxide, generally TiO₂.

High sensitization of the mesoporous metal oxide structure (i.e. loading of QDs) while maintaining the quantum confinement is important for efficient QDSSC operation. Two solution-phase approaches to QD deposition are commonly used: (i) direct growth of quantum dots onto the mesoporous metal oxide by introduction of cationic and anionic species sequentially, e.g., successive ionic layer adsorption and reaction (SILAR),^{64, 65} or via chemical bath deposition (CBD),^{66, 67} and (ii) direct absorption of pre-synthesized colloidal quantum dots using bifunctional organic linker molecules.^{68, 69} The first approach involves nucleation and growth onto the mesoporous metal oxide surface, leading to a higher effective coverage. However, these methods lack control of crystallinity and size. Furthermore, the surface tension and viscosity of the solvent can make it difficult for the ions to reach deep into the mesoporous film, causing an inhomogenous loading of QDs. The second approach with pre-synthesized quantum dots provides precise control of size and size distributions of QDs, but often leads to a lower

loading of quantum dots, even in the case of applied external electric fields.⁷⁰ Lastly, solution-phase reactions are more likely leave behind impurities from reaction by-products. For these reasons, the utility of solution-phase QD deposition may be limited. One method to improve upon these techniques is through gas-phase deposition by taking advantage of enhanced transport of gaseous materials through porous structures and eliminating issues related to surface tension and slow diffusion in liquids. A gas-phase process capable of infiltrating porous substrates with fine control over deposition thickness is sought to improve upon these solution-phase techniques. ALD is one such approach that has been explored recently.

ALD is primarily used to grow ultrathin films with high conformality and uniformity by taking advantage of the sequential, self-limiting gas-surface reaction process. However, under some conditions it can also be used to grow nanoparticles, including QDs.^{71, 72} Earlier work from our group by Brennan *et al.*⁷³ showed that ALD led to deposition of different sizes of quantum dots by limiting the growth to within the ALD nucleation regime. In that work, CdS quantum dots were grown on both flat and mesoporous TiO₂ substrates. The growth rate of CdS showed two significantly different regimes as illustrated in Figure 3a. The nucleation period for the first 20 cycles had a growth rate of only ~ 0.2 Å/cycle, followed by a standard growth regime with a higher growth rate of ~ 1.3 Å/cycle. During the nucleation period, island growth of CdS takes place, leading to formation of discrete particles that eventually coalesce into a continuous film once the growth approaches the steady state regime. If the sizes of these islands can be controlled within the Bohr excitonic radius of the material (5.6 nm for CdS), they will exhibit quantum confinement effects. In this study, within the first 5 cycles of the nucleation period, a low density of CdS QDs with diameters ~ 1 -4 nm was observed. Both the areal density and size of CdS QDs increased with ALD cycle numbers, with the size of the CdS nanoparticles after 10 cycles varying between ~ 2 -10 nm as shown in Figure 3b. Growth at a limited number of nucleation sites during the nucleation regime results in the formation of individual quantum confined nanoparticles. The controlled ALD growth can then be used for size optimization of these nanoparticles at the nucleation sites.⁷¹

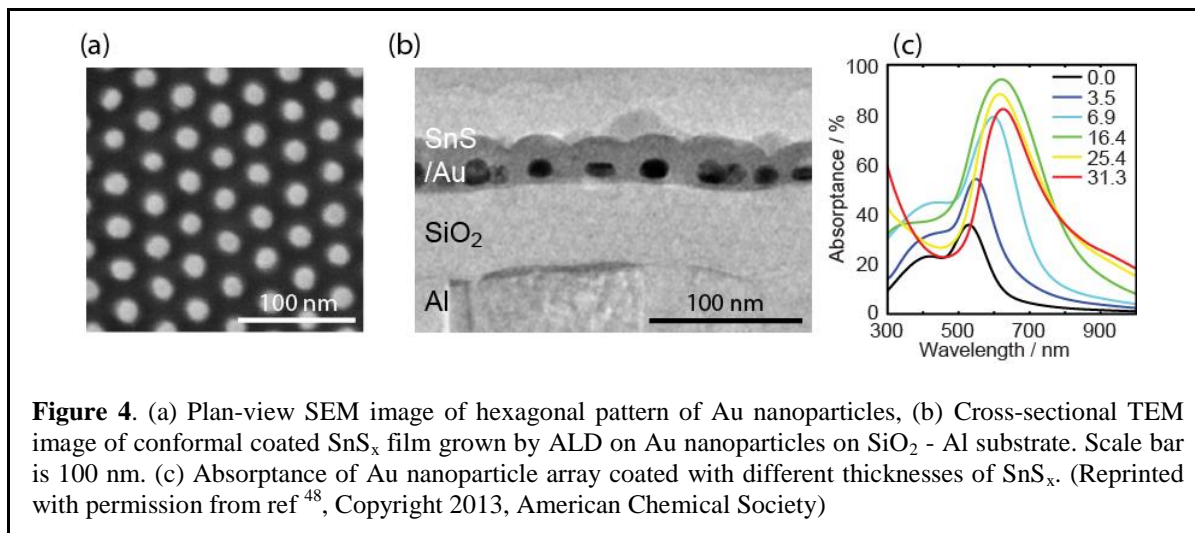
In the same work,⁷³ Brennan *et al.* reported solid-state PV devices on mesostructured TiO₂ sensitized by ALD-grown CdS QDs. A systematic red-shift in the UV-Vis absorption edge was observed with increased ALD cycles, which is due to the size quantization effect. The overall PV performance, as shown in Figure 3c, strongly depended on the number of ALD cycles employed for deposition of QDs. The short-circuit current (J_{SC}) increased with increasing number of ALD cycles up to 5 cycles, followed by a decrease with further ALD cycles. This effect may be related to the aggregation of CdS QDs leading to a lower electron injection rate to TiO₂. A maximum power conversion efficiency of 0.25 % was observed for 5 ALD cycles. In addition, PbS QDs grown by ALD on mesoporous anatase TiO₂ were also reported.⁷⁴ The sizes of the PbS QDs after 10 cycles were distributed from 2.8 to 4.8 nm and the coverage of PbS QDs on the mesoporous TiO₂ was uniform (Figure. 3d). A total power conversion efficiency of 0.3 % was observed on such ALD-PbS sensitized solar cells.



3.1.2. Plasmonic solar cells

For many applications, including solar energy conversion to fuel and electricity, it is desirable to minimize the amount of light absorber material. Thinner light absorbers can reduce cost by using less material, and if the thickness of the absorber layer is less than or comparable to the mean free path of the charge carriers and/or the diffusion length of excitons, recombination within the light absorber layers can be minimized, thus improving the overall power conversion efficiency. The light absorption of a material is characterized by the absorption coefficient (α) of the material. By making a material thicker than its characteristic absorption length ($1/\alpha$), it is possible to absorb essentially all the light that enters the material. Increasing the absorption coefficient of a material will reduce the required thickness of the light absorber without compromising its ability to capture and convert solar energy.

One way to minimize the amount of material needed for high light absorption is to use a plasmonic structure, as it offers a means to achieve light concentration in ultrathin absorber layers. Novel designs based on plasmonic absorber/spacer/reflector configurations have been used to harvest light both in the visible⁷⁵ and IR regions.⁷⁶



By combining metallic plasmonic nanostructures with semiconductors, our group has recently reported a record effective absorption coefficient in gold nanoparticles surrounded by a dielectric film.⁴⁸ The structure that allowed for extreme visible light absorption, shown in Figure 4a, was enabled by ALD. The plasmonic absorber layer consisted of a dense hexagonal gold nanoparticle array, with an average lattice spacing of 37.9 nm, that was lithographically prepared over micrometer domains using unidirectional self-assembly of block copolymers. This plasmonic absorber layer was prepared on a SiO_2 layer which acted as a spacer between the plasmonic absorber and a reflecting aluminum film below the SiO_2 . Using ALD, the plasmonic absorber layer was subsequently coated with three different semiconductors; SnS_x , ZnO and Al_2O_3 . The ALD processes resulted in uniform and circumferential coating of the semiconductors around the gold nanoparticles as shown in the cross sectional TEM image in Figure 4b. The growth of these semiconductors by ALD allowed thickness control down to the atomic scale. These ultra-thin semiconductor films on the plasmonic arrays did not show any significant absorption themselves but improved the absorbance of the plasmonic array. The absorbance of the overall plasmonic array increased with the thickness of SnS_x , up to 94.2 % at a wavelength of 619 nm for a 16.4 nm thick SnS_x coating (Figure 4c) No other deposition technique has such precise and uniform control over the thickness at this length scale. Finite element method calculations suggested that almost 93% of the light was absorbed within the metallic gold dot array. Since the volume of the gold array is equivalent to a film with thickness of only 1.6 nm, the effective absorption coefficient of this noble structure was calculated to be a record-high value of $1.7 \times 10^7 \text{ cm}^{-1}$.

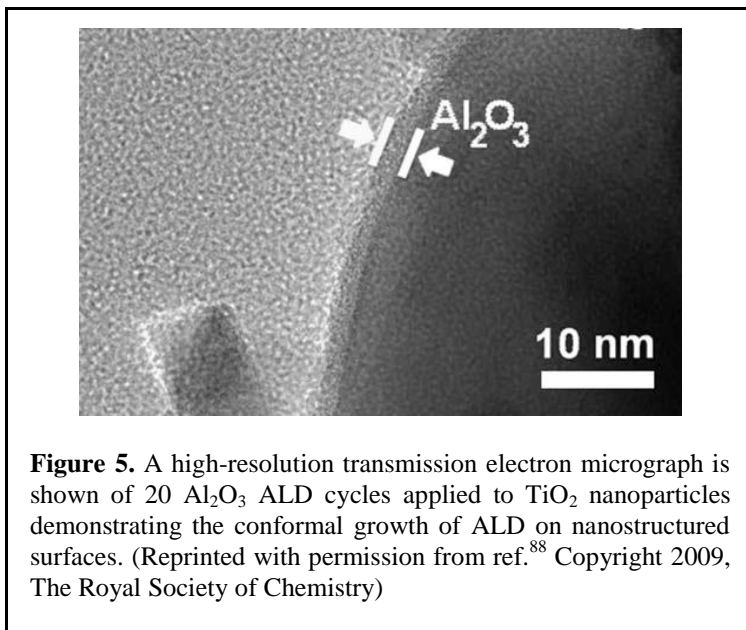
More recent studies in our group are exploring ALD of absorbing semiconductors within the Au plasmonic array. Initial results show that this enables strong coupling of the localized surface plasmon resonance of the array with the semiconductor and can lead to an average absorption in the ultrathin coating that is comparable to 100-fold thicker solar cell absorbers.⁷⁷

3.2 Recombination Barrier Layers

3.2.1 Dye-sensitized Solar Cells

Solid-state DSSC performance has yet to reach that of liquid cells due in part to relatively poor hole mobility in solid state HTMs, incomplete pore filling, poor charge collection and high recombination rates between the metal oxide and solid-state HTM.^{29, 78, 79} The electron transfer step in many solid-state HTMs, such as spiro-OMeTAD (2,2',7,7'-tetrakis-(N,N-di-*p*-methoxyphenylamine)-9,9'-spirobifluorene), involves a single electron transfer as opposed to a multistep process in the I/I_3^- redox couple, resulting in faster recombination processes observed in solid-state HTM devices.^{80, 81} A review of charge transport and recombination processes in DSSCs can be found in reference⁸². The dominant charge recombination in spiro-OMeTAD based devices (and most DSSCs that do not employ the I/I_3^- electrolyte) is the back reaction of electrons from the TiO_2 with holes from the HTM.⁸³ It was shown by O'Regan and Lenzmann that in CuSCN solid-state DSSCs, recombination rates are between 10 times (at open circuit voltage) and 100 times (at short circuit) faster than in equivalent devices with iodide redox couple liquid electrolyte. The increase in recombination was determined to be the key role in limiting fill factors in solid-state DSSCs, which would need to be overcome to achieve a competitive solar technology.⁷⁸ Importantly, recombination processes limit solid-state device thicknesses to $\sim 2 \mu m$ ⁸⁴ (relative to $\sim 7 \mu m$ in liquid cells),²² preventing complete light absorption and restricting overall cell efficiency. This has led to studies on barrier layers to block the back recombination process while still allowing for sufficient rates of both electron injection from the dye excited state into the TiO_2 and dye regeneration from the HTM after electron injection.

Three possible effects are expected from the application of a barrier layer: (1) the formation of a tunnel barrier for which an electron in the metal oxide can recombine with a hole in the HTM only by tunneling through the barrier layer, (2) a surface dipole effect, changing the distribution of charge at the metal oxide interface and creating an electric field that shifts the band offset between the dye and metal oxide, and (3) passivation of surface states, resulting in a lower density of states existing near open circuit voltage (V_{oc}).⁸⁵ These effects are not mutually exclusive. Effect (1) is expected to decrease the recombination rate constant and, if we assume electron injection into the dye is not significantly affected, V_{oc} will increase due to a higher electron concentration under illumination, resulting in larger quasi Fermi-level splitting. Effects (2) and (3) will increase V_{oc} via band offsets, but not recombination rates at V_{oc} because the recombination pathway is not surface state limited.⁸⁶ Palomares et al. first investigated SiO_2 , Al_2O_3 and ZrO_2 as metal oxide barrier layers on top of mesoporous TiO_2 by sol-gel deposition, observing that Al_2O_3 had the best barrier layer performance.⁸⁷ Further studies were done with solution-phase Al_2O_3 deposition, demonstrating that Al_2O_3 behaved as a tunnel barrier and could improve the V_{oc} , fill factor and performance of mesoporous TiO_2 based solar cells with a solid-state HTM.⁸⁵ One observation from these studies was that there was variability in the Al_2O_3 deposition and lack of thickness control, potentially due to adsorbed moisture, ambient humidity and moisture in the alkoxide organic solutions.



grow at as low as 33 °C.⁸⁹ In the ALD Al₂O₃ barrier layer work done by Lin et al.⁸⁸ one cycle of Al₂O₃ could improve the power conversion efficiency of DSSCs by 14 %. At higher cycle numbers, the Fermi level of the TiO₂ was increased above the lowest unoccupied molecular orbital of the dye molecule, blocking electron injection and ruining device performance. Several authors have reported efficiency improvements after implementing barrier layer materials in both liquid and solid-state DSSCs; however, there is a large discrepancy as to what the optimal thickness should be with ALD reports ranging from 1 to 20 ALD cycles (0.1 to 2.0 nm).^{88, 90-93 94} These discrepancies may be the result of incomplete pore infiltration, variations in dye LUMO levels relative to TiO₂, or different surface pre-treatments prior to barrier layer deposition.

One surface treatment that has been demonstrated to have advantageous effects on DSSC performance is the deposition of amorphous TiO₂ via an aqueous TiCl₄ solution,⁹⁵ which was observed to decrease interfacial recombination at low deposition thicknesses.⁹⁶ Our group investigated the effect of Al₂O₃ barrier layers on TiO₂ based DSSCs by comparing the Al₂O₃ ALD to this TiCl₄ solution surface treatment.⁷⁹ We showed that while Al₂O₃ behaves as would be expected of a barrier layer material in terms of open circuit voltage, short circuit current, and dependence of electron lifetime on barrier layer thickness, efficiency enhancements were only observed at one ALD cycle and no enhancement was observed when ALD was applied to TiCl₄ treated devices. In fact, at one cycle, the DSSC device performed similarly to the TiCl₄ treated device. At one cycle, the Al₂O₃ film is still within the nucleation growth regime and has yet to form a complete film. Calculations have predicted the surface coverage of a single ALD cycle of Al₂O₃ to be 50-75 % on mesoporous TiO₂.⁹⁷ This suggests that Al₂O₃ nucleation may occur on “problem sites” on the TiO₂ surface that resist dye adsorption, electron injection or have higher surface recombination than typical TiO₂ surface sites (i.e. these problem sites do not have a positive contribution to overall current). As such, ALD of Al₂O₃ offers

Atomic layer deposition (ALD) provides an alternative approach to barrier layer formation. It enables precise investigation of barrier layer effects on DSSCs with angstrom level thickness control and enhanced infiltration capabilities relative to sol-gel processes, ensuring uniform deposition on nanoporous substrates. Figure 5 shows a conformal, 2 nm thick coating of Al₂O₃ on TiO₂ nanoparticles from 20 cycles of trimethylaluminum and water as ALD precursors at 150 °C,⁸⁸ although Al₂O₃ can

an alternative method of improving device performance when TiCl_4 treatment is not possible for DSSCs.

The Al_2O_3 work motivated studies on alternative barrier layer materials that are more conductive and have slower growth rates (less than $1 \text{ \AA}/\text{cycle}$) for finer tuning of barrier layer thickness. One such system is the ALD growth of In_2O_3 using trimethylindium (TMI) and water as the precursors ($0.4 \text{ \AA}/\text{cycle}$).⁹⁸ Our studies of In_2O_3 barrier layers⁹⁹ have demonstrated that this system exhibits barrier layer effects 1 and 2 (described previously), with V_{oc} improvements up to the first 20 ALD cycles ($\sim 8 \text{ \AA}$) due to both recombination suppression and TiO_2 conduction band modulation via surface dipole effects. The combination of these effects resulted in V_{oc} improvements of over 100 mV with a near record V_{oc} performance at 1.00 V. This observed surface dipole effect was shown to reverse at thicker In_2O_3 films (30 ALD cycles, $\sim 12 \text{ \AA}$), in turn resulting in a negative effect on the device V_{oc} .

3.2.2 Quantum Dot Sensitized Solar Cells

The QDSSC structure is similar to that of DSSCs with the exception of QDs acting as the sensitizer. This makes QDSSCs a logical system for the application of ALD barrier layers. One key difference between the two systems is the higher thermal and mechanical stability of the QD sensitizers relative to dyes; however, this comes at the expense of surface coverage, which is generally poorer for the QDSSCs. Two important consequences arise in QDSSCs: first, there is a direct TiO_2/HTM interface not seen in the DSSCs and second, the enhanced stability of QDs allows for the ALD deposition of barrier layers subsequent to the sensitizer deposition.

Our group applied barrier layers to QDSSC devices and found that excited state electron lifetimes increased due to reduced recombination rates (Figure 6a) as expected from the DSSC literature. Furthermore, we explored two QDSSC barrier layer structures illustrated in Figure 6b: $\text{TiO}_2/\text{QD}/\text{Al}_2\text{O}_3$ and $\text{TiO}_2/\text{Al}_2\text{O}_3/\text{QD}$ where the barrier layer is deposited either before or after the quantum dot sensitizers. QDSSC devices based on both CdS and PbS QDs were investigated. In these studies, the CdS was deposited by successive ionic layer adsorption and reaction (SILAR) while the PbS was deposited *in-situ* via ALD as described in Section 3.1.1. These studies showed that Al_2O_3 grown prior to QD deposition reduced recombination between the TiO_2 and both oxidized quantum dots as well as the HTM. Al_2O_3 deposition after the QD only reduced recombination between the TiO_2 and HTM; however, both configurations resulted in increased excited state electron lifetimes.

The *in-situ* deposition of both barrier layer and light absorber via ALD,⁷⁴ as carried out for the PbS QDSSC system, allows for barrier layer studies in which the chances of surface contamination are minimized because vacuum processes are used for both steps. For these PbS *in-situ* devices, it was shown that the presence of Al_2O_3 did not affect the ALD PbS nucleation (Figure 6c) and that the barrier had a large effect on carrier collection efficiency across a wide spectral range (Figure 6d), ultimately leading to a nearly two-fold enhancement of device performance for the $\text{TiO}_2/\text{Al}_2\text{O}_3/\text{PbS}$ configuration relative to the control TiO_2/PbS device.

In addition to the Al_2O_3 barrier layers, a multitude of other ALD systems have been studied for barrier layer applications. Many of these studies are summarized in Table 1. What is clear is that surface barrier layers have a significant effect on device operation with strong dependencies on sub-nanometer film thicknesses. The unparalleled conformality achieved in deposition on nanostructured surfaces, the high resolution in film thickness, and the ability for fully *in-situ* device fabrication make ALD ideally suited for the application of barrier layers on sensitized solar cell structures.

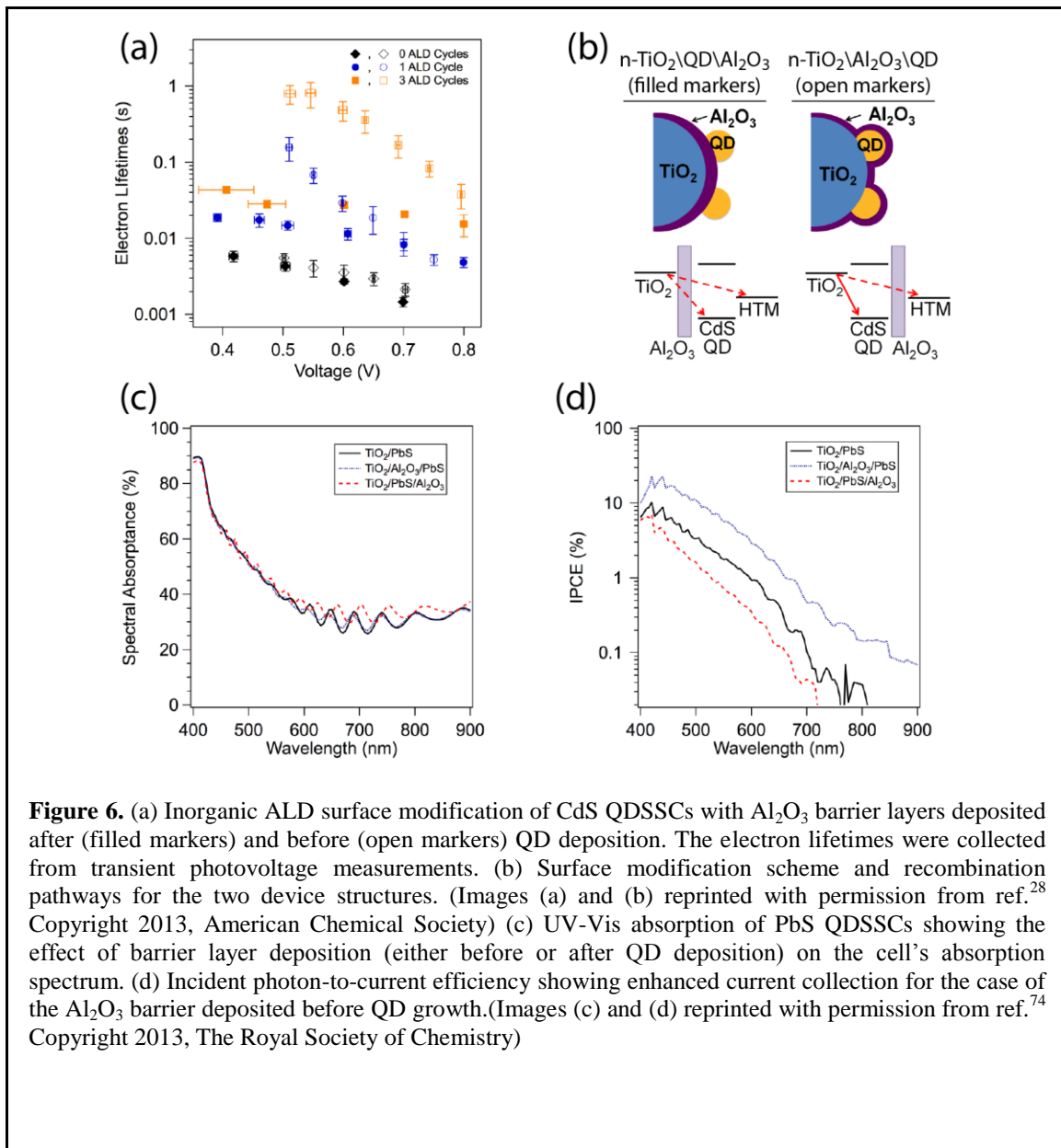


Figure 6. (a) Inorganic ALD surface modification of CdS QDSSCs with Al_2O_3 barrier layers deposited after (filled markers) and before (open markers) QD deposition. The electron lifetimes were collected from transient photovoltage measurements. (b) Surface modification scheme and recombination pathways for the two device structures. (Images (a) and (b) reprinted with permission from ref.²⁸ Copyright 2013, American Chemical Society) (c) UV-Vis absorption of PbS QDSSCs showing the effect of barrier layer deposition (either before or after QD deposition) on the cell's absorption spectrum. (d) Incident photon-to-current efficiency showing enhanced current collection for the case of the Al_2O_3 barrier deposited before QD growth. (Images (c) and (d) reprinted with permission from ref.⁷⁴ Copyright 2013, The Royal Society of Chemistry)

Table 1. Summary of ALD systems reported in literature for barrier layer applications in DSSC and QDSSC devices.

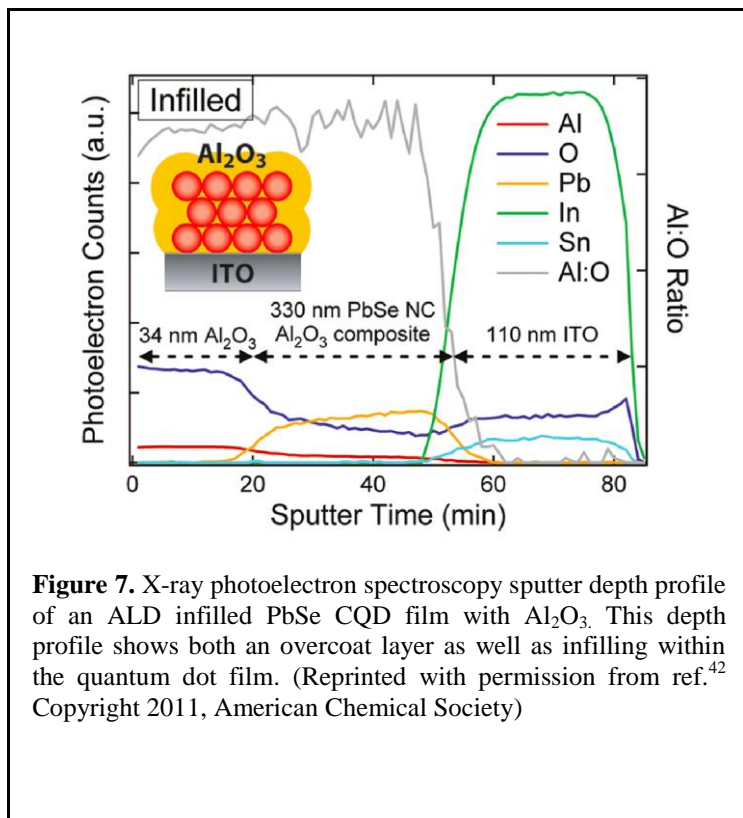
ALD System	References
Al ₂ O ₃	28, 74, 79, 88, 90, 92, 97, 100-108
HfO ₂	100, 109
ZrO ₂	93, 110
TiO ₂	91, 103, 111
Ga ₂ O ₃	110, 112
In ₂ O ₃	99
Nb ₂ O ₅	110
Ta ₂ O ₅	110

* Indicates QDSSC devices

3.3 Colloidal Quantum Dot Infiltration

Infilling of CQD films refers to the deposition of materials within the quantum dot matrix. Infilling is desirable in CQD films because it can passivate QD surfaces, reduce energetic barriers to charge transport, and stabilize the film from oxidation as well as thermal and mechanical degradation. ALD provides a superior method for infilling CQD films because of its ability to conformally coat highly porous structures. A depth profile of a CQD device after ALD infilling⁴² is shown in Figure 7. The uniform profile of the ALD Al₂O₃ throughout the PbSe CQD layer is apparent. The infilling must be done at relatively low temperatures to avoid sintering of the nanoparticles, an effect driven by the reduction of surface energy occurring at temperatures below bulk melting temperatures. This is especially true when the QDs have undergone ligand exchange with short chain ligands for improved CQD carrier transport, as is the case in most CQD solar devices.¹¹³ TEM annealing experiments have shown hexylamine-capped PbSe QDs to rotate, translate and sinter at temperatures as low as 100 °C under vacuum.^{114, 115} For this reason, infilling is restricted to low temperature ALD systems.

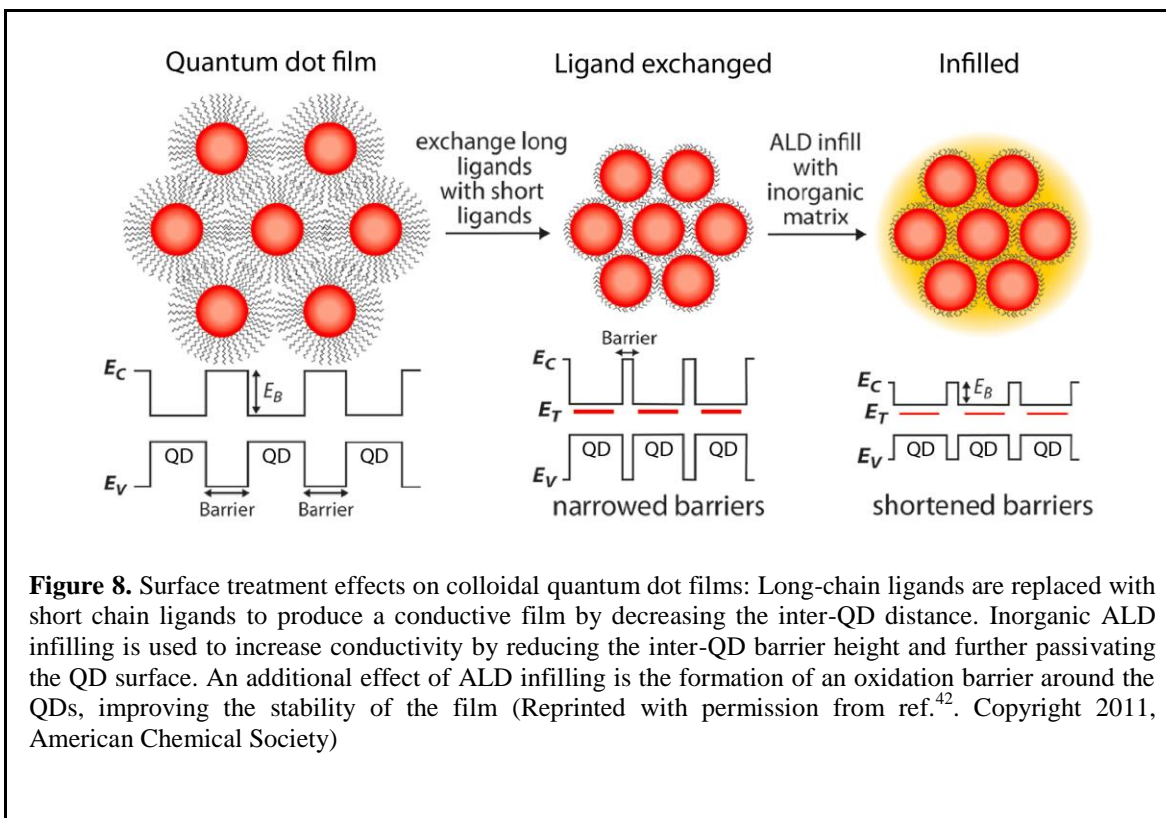
Pourret et al. performed one of the earliest quantum dot infilling studies, with the infiltration of CdSe QD films with ALD ZnO.¹¹⁶ The authors measured ALD precursor (diethyl zinc) uptake into the CdSe QD film *in-situ* with a quartz crystal microbalance and found that long chain hydrocarbons reduced ALD infiltration capabilities by blocking interstitial voids in the film and hindering precursor diffusion. An ammonium hydroxide treatment was able to strip ligands from the film, which significantly improved diethyl zinc uptake. ZnO deposition in the CdSe film was shown to increase carrier mobility by a staggering 2-3 orders of magnitude while simultaneously improving the mechanical stability of the CdSe film.



carrier mobility; however, Liu et al. showed that ligand exchange may not be sufficient at passivating QD surfaces and further improvements can be achieved through inorganic infilling with ALD Al₂O₃.^{42, 120} Combinations of inorganic ligand exchange and ALD Al₂O₃ infilling have been used to improve electron mobilities in PbSe¹²⁰ and PbS¹²¹ colloidal quantum dot films. In addition to charge transport effects, mid-gap states that arise from QD surface states affect the V_{oc} achievable in CQD devices through Fermi level pinning at the QD-metal interface. The removal of mid-gap states through improved passivation and composition control has been shown to reduce recombination rates and enhance the V_{oc} of CQD solar cells.^{122, 123} Similar effects have been demonstrated on other electronic materials, including c-Si solar cells,¹²⁴ copper indium gallium selenide (CIGS) solar cells¹²⁵ and InGaAs field effect transistors.¹²⁶ While this V_{oc} enhancement was not accomplished through ALD, it suggests that passivation effects from ALD infilling may lead to improved cell voltages in certain instances.

Electronic properties of semiconductors depend greatly on the presence or absence of electronic states near the band gap. Two such properties important to colloidal quantum dot devices are charge transport and device open circuit voltage. Surface states are known to exist within the band gap of lead chalcogenide quantum dots.¹¹⁷ These surface states can dictate overall transport properties of the QD film, generally resulting in poor solar performance.^{118, 119} Organic and inorganic ligand exchange strategies have been used to passivate these surface states and improve

Charge transport does not solely depend on electronic trap states, but rather also depends on inter-QD barriers in the case of colloidal quantum dot films.¹²⁷ The width and height of inter-QD barriers are important to carrier transport within CQD films and, in conjunction with mid-gap states, determine film mobilities. Short chain ligand and halide ion exchange methods have been used to decrease the width of inter-QD barriers; however, these ligand exchanges do not necessarily lower the barrier height. ZnO ALD infilling has been shown to selectively improve electron mobility by a factor of 17 in the case of PbSe CQD films⁴² due to a ZnO conduction band that lies within 0.1-0.4 eV of the PbSe 1S(e) level.^{128, 129} The effect of ligand exchange followed by ALD infilling is shown in Figure 8.



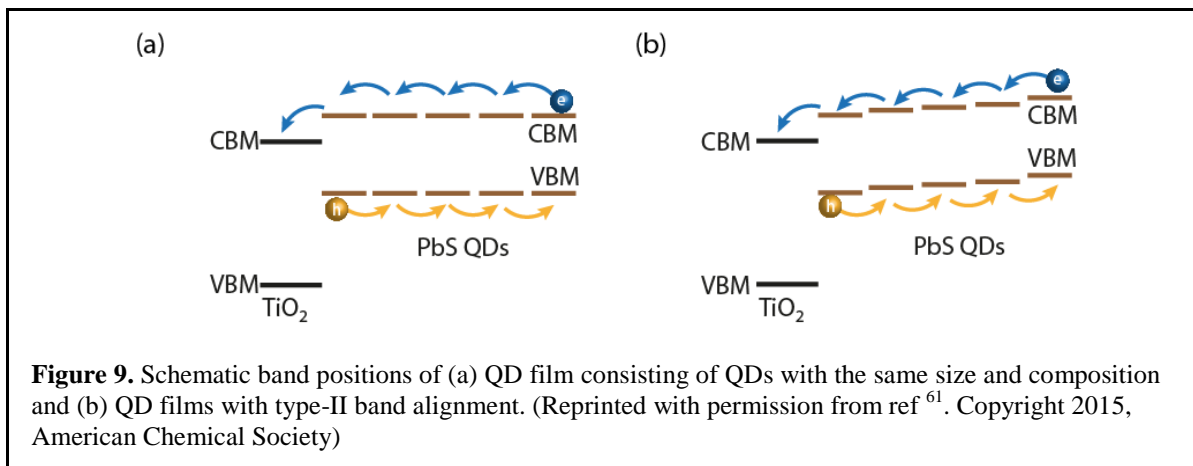
Another area of importance for CQD devices is stability. The high surface area to volume ratio of QDs makes these materials inherently meta-stable and is a major concern for the extended stability under real world conditions required for the commercialization of CQD photovoltaics. The oxidation process for lead chalcogenides, well explained elsewhere,^{113, 130} is especially severe for PbSe QDs which are observed to irreversibly oxidize and lose photovoltaic activity with air exposure in a matter of minutes.⁴² The rapid degradation of PbSe in air is a challenge for commercialization, but beneficial from the perspective of stability studies. Passivation and encapsulation are ways of protecting colloidal films and both can be achieved through ALD. Liu et al. established Al₂O₃ encapsulation via ALD as a method for CQD film stabilization in which PbSe CQD solar cells were stable in air for months with no signs of oxidation.⁴² This encapsulation scheme involved two parts: a 2-3 nm Al₂O₃ infilling layer and a ~30 nm Al₂O₃ overcoat layer (Figure 7). Both the infilling and overcoat served specific purposes towards device

enhancement: where the overcoat acted as a gas diffusion barrier, greatly slowing oxidative degradation, the infilling improved performance through carrier mobility enhancement via trap passivation and V_{oc} improvements, likely from higher built-in voltages at the QD/Schottky contact. The authors note that the metal contact was deposited before the overcoat layer was applied and that Ag evaporation has been shown to penetrate the 2-3 nm Al_2O_3 shell to form a direct contact with the QDs and experience low series resistance.

It was previously mentioned that quantum dots are promising third generation absorber materials and one reason for this is the prospect for carrier multiplication (CM), also known as multiple exciton generation. CM is a way to utilize excess energy created by the absorption of a photon with energy beyond twice the band gap energy (E_g) of the semiconductor, and it has been put forth as a way to break the Shockley-Queisser limit.^{131, 132} It refers to the formation of multiple excitons by a single photon. Despite initial reports of high quantum yields from carrier multiplication in nanocrystals^{63, 133} it is now generally accepted that nanocrystals do not inherently have higher CM yield than in bulk.^{134, 135} While this dims the prospect of large efficiency gains in lead chalcogenide devices, which in bulk have relatively poor CM efficiency, quantum confinement can be important for tuning the bandgap of other materials with higher CM efficiencies.¹³⁶ CM in quantum dots results in charges in close proximity, with rapid recombination rates due to Auger recombination; therefore, to be useful for photovoltaics, charge transport must be sufficiently fast to collect charges before recombination.¹³⁷ The charge transport enhancement from ALD infilling has been shown to activate CM in PbSe CQD films, leading to CM efficiencies near that of bulk material with minimal Auger recombination.¹³⁸ Although high efficiency photovoltaics resulting from CM has yet to be observed, this work on PbSe demonstrates that a technique like ALD may allow CQD films to take advantage of quantum confinement without necessarily losing CM properties.

3.4 Non-ALD Surface Modification

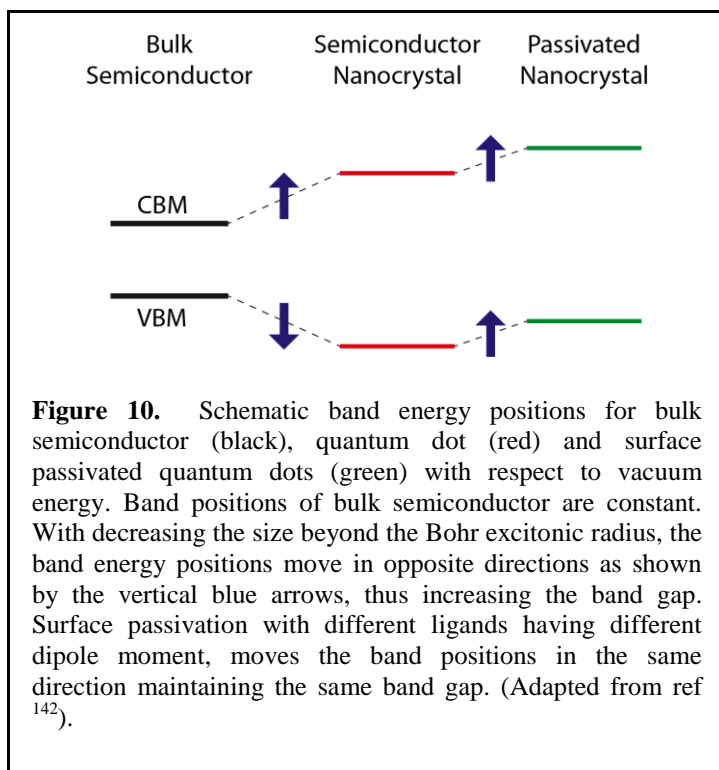
Charge transport at the maximum power point is of paramount importance for the performance of CQDSCs. In the previous section, we have discussed some strategies to improve the charge carrier mobility through surface passivation by infilling of QDs using ALD. An alternative approach is to increase the width of the depletion region where drift current dominates charge transport. In this section, we will discuss how band alignment of quantum dots by passivating ligands can extend the depletion region within the CQD films. In general, ALD processes are not capable of altering the passivating ligands around the QD; hence, more traditional ligand exchange processes, as described below, provide a means of tuning the organic groups around the QD. A process related to ALD, that of molecular layer deposition (MLD), may find use in the future for achieving similar organic modification of QD particles, but has not yet been applied for this application.



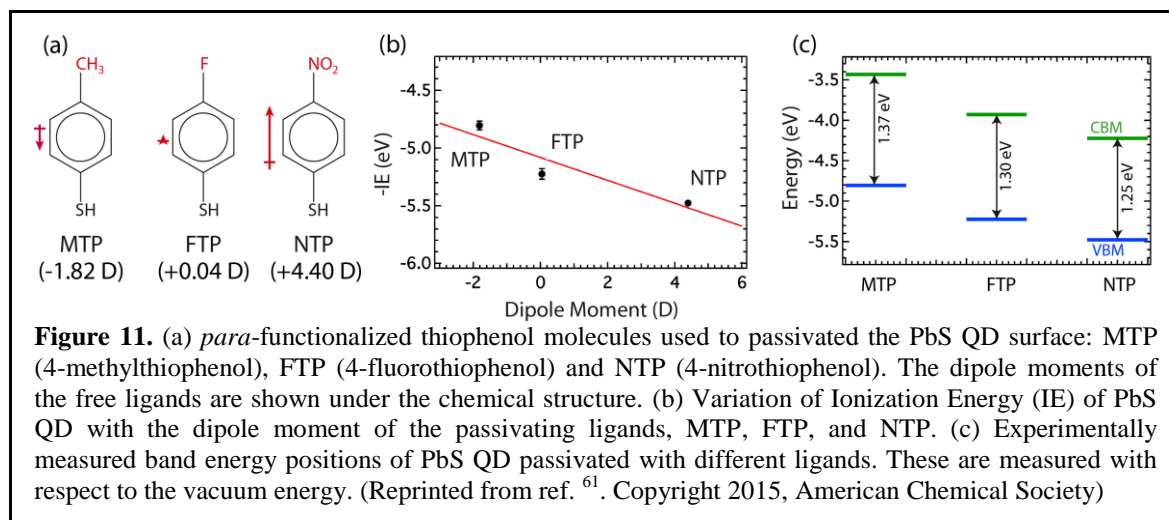
In a typical CQD solar cell, the size and composition of each quantum dot is kept almost identical, which leads to an energy diagram of the solar cell as shown in Figure 9a. Band engineering of these CQD solar cells is possible. The band positions of quantum dots can be tuned through the passivating ligand dipole moment in such a way that they form a type-II band alignment with each other (Figure 9b). This particular band alignment will also create an effective electric field, which will in turn enhance the depletion region and the directionality of the charge transport, thereby reducing recombination losses.

In this context, band positions can be altered in a few different ways. In general, the conduction band minima (CBM) and valence band maxima (VBM) are mainly contributed by the cation *s*-orbital and anion *p*-orbitals, respectively. By changing the size of a quantum dot below its Bohr excitonic radius, it is possible to alter the CBM and VBM positions. However, by decreasing or increasing the size of the quantum dot, both CBM and VBM move in opposite directions thus increasing or decreasing the bandgap, respectively. Hence size variation does not lead to a type-II band alignment between quantum dots having the same composition. The band positions and band gap of a ternary-alloyed semiconductor can also be altered with its chemical composition within the band gap of the two extreme compositions. This strategy might create a type-II band alignment.

A third strategy—that of surface ligand modification—can be used to specifically create type-II band alignment in a CQD film. Earlier, it was shown that a self assembled monolayer of organic molecules with sufficient dipole moment on metal or semiconductor surfaces can alter the ionization potential of the materials.¹³⁹⁻¹⁴¹ Essentially, all colloidal quantum dots require organic ligand molecules on their surface as the passivating layer. By altering the dipole moment of these ligand molecules, it is possible to control the electronic structure of the quantum dots. The electric field generated due to the dipole moment of the ligands operates with the same strength on both CBM and VBM, thus changing both band positions in the same direction unlike the size variation, as explained in Figure 10.



dipole moment of the free ligand molecule, suggesting a direct effect of the dipole moment on the electronic structure of the quantum dot. Moreover, the experimentally measured band positions of PbS QDs with different passivating ligand molecules showed a type-II band alignment as shown in Figure 11.

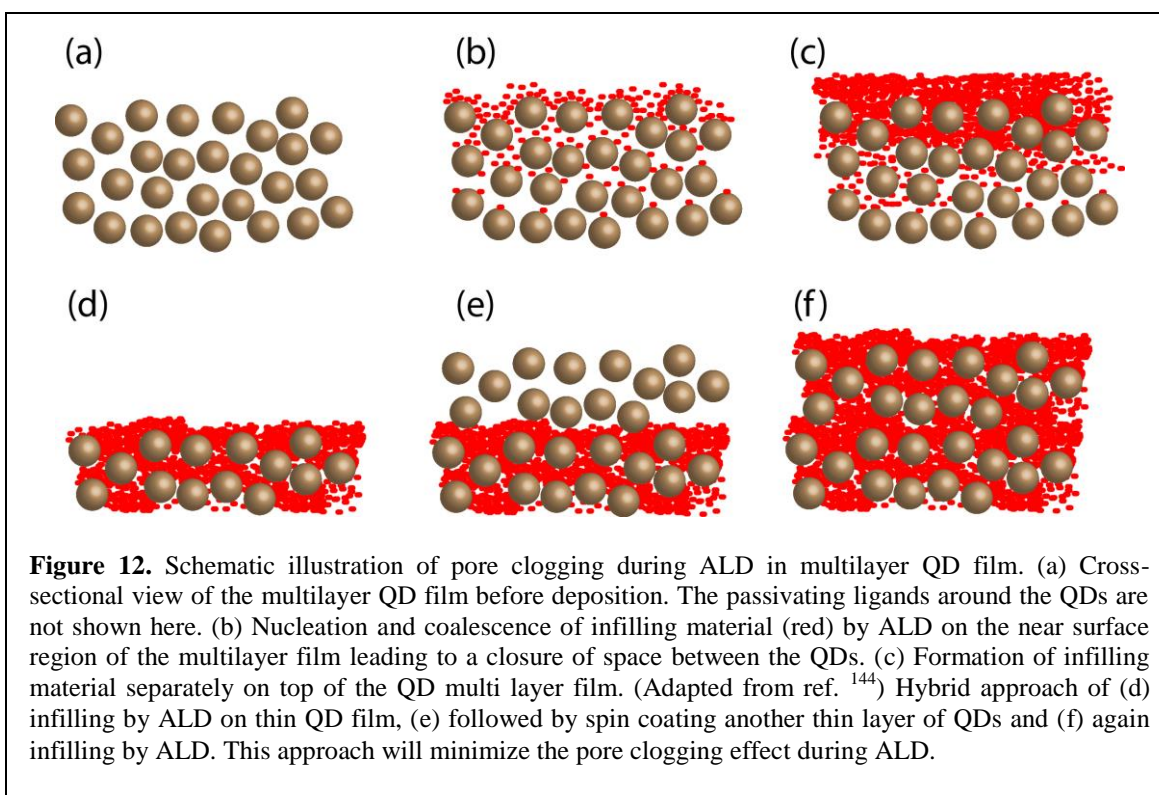


The use of these band engineered PbS QDs allowed for the fabrication of photovoltaic devices having a type-II band alignment, referred to as a *unidirectional* configuration. This configuration showed higher photocurrent and fill factor compared to the *control* configuration where all quantum dots are essentially identical. In recent work¹⁴³ by Bawendi et al., the band positions of PbS quantum dots were altered in a similar fashion using tetrabutylammonium iodide (TBAI) and 1,2-ethanedithiol (EDT).

As EDT shifts up both the band positions (CBM and VBM) compared to TBAI ligand, a type-II band alignment is thus achieved by replacing the top two PbS-TBAI with PbS-EDT. Photovoltaic devices with this configuration also showed improvement, reaching a notable total power conversion efficiency of 8.5 %.

4. Outlook

In this review, we discussed different applications of ALD for nanostructured photovoltaic applications. These applications encompass development of several different aspects of nanostructured photovoltaics. For example, ALD has found use in forming barrier layers, passivation layers, and even absorber layers in various PV structures. First, in QDSSCs, ALD has been used to grow different QD sensitizers with controlled size. In addition, highly conformal and precisely thickness-controlled semiconductor films grown by ALD on plasmonic nanostructures have helped achieve absorption coefficients as high as $1.7 \times 10^7 \text{ cm}^{-1}$. Second, we described how ALD can address the recombination issues common in DSSCs and QDSSCs by growing barrier layers with thickness on the order of sub-nanometers. Third, we discussed the use of ALD to infiltrate multilayer CQD solar cells with different dielectric materials to passivate the QDs as well as to improve the charge carrier mobilities of the multilayer QD films. In each of these applications, comparable techniques such as CBD, CVD, or physical vapor deposition (PVD) typically cannot provide same level of control over the material growth and conformality, which are crucial for the development of the nanostructured photovoltaics.



Despite its many advantages, there are also challenges and possible pitfalls in the use of the ALD technique for nanostructured photovoltaics. One limitation is temperature. Most of the ALD processes operate at high temperatures. Due to high surface-to-volume ratio, nanoparticles exhibit significant melting point depression¹⁴⁵ which is further aggravated by the vacuum inside the ALD reactor chamber. It is possible to form a film from multilayer nanoparticles at relatively low temperature and hence lose quantum confinement behavior in CQD solar cells. To prevent this, it is necessary to perform ALD at low temperatures. The ALD temperature window depends on the reactivity and thermochemistry of the precursors. In several cases, low temperature ALD deposition yields amorphous material.⁵¹ Recent advances on spatially selective atmospheric ALD¹⁴⁶ may help in preventing the melting of nanoparticles because vacuum, which suppresses QD melting/sintering temperatures due to ligand desorption, is not used. Another potential solution is to deposit a barrier layer materials such as Al₂O₃ that can be grown at low temperature around the QDs, followed by deposition of second materials at higher temperature. The thin barrier layer grown at low temperature should decrease the melting of the QDs.

A second challenge is inhomogeneous infilling of certain porous structures such as multilayer QD films using ALD. Due to the replacement of the native long-chain passivating molecules by small molecules around the QD for CQD photovoltaic systems, the interparticle distance decreases significantly in the multilayer QD film. While “true” ALD would produce homogeneous films, this can be difficult to achieve in practice when depositing on extremely high aspect ratio substrates or tortuous nanoporous films. Under these conditions, precursor exposure must be increased to allow for diffusion and often “true” ALD is not feasible. In these films, the infilling of such sub-nanometer pores by ALD can lead to non-uniform growth along the depth of the multilayer QD film as shown in Figure 12a-c. However, it is possible to overcome infiltration issues by using new strategies. One potential hybrid approach is sequential deposition of a thin layer of QDs on a substrate, followed by an infilling using ALD, as shown schematically in Figure 12d-e. This process can then be repeated until the desired thickness of the multilayer QD film is achieved. This hybrid method should minimize the inhomogeneity along the depth of the multilayer QD film. Other challenges in the application of ALD for PV include potential difficulties controlling ALD nucleation, and the need for a broader spectrum of ALD precursors. Regarding the first point, in some cases¹⁴⁷, ALD grows island type materials due to poor nucleation, whereas a thin uniform and continuous layer of material is necessary in several applications. Furthermore, commercial availability of precursors needed to grow certain materials limits the application of ALD for such materials¹⁴⁸.

Despite the limitations, ALD is likely to be of significant importance in improvement of nanostructured photovoltaics. As ALD has already been established as an excellent technique to modify surfaces, it sits poised to play a key role in the development of any nanostructured solar cells which possess high surface area. Here we suggest two areas for future impact. One example is the organolead halide perovskite systems. Over the last few years, the total photovoltaic performances of the organolead halide perovskite absorbers have reached 20.1 %.¹⁴⁹ These perovskite solar cells have been reported both in sensitized mesoporous and thin planar device architectures, which

are similar to QDSSCs and CQD solar cells, respectively. While a majority of the studies report on the development of the absorber layer and its stability and structure, only a few studies have reported on interfacial effects in such solar cells. Some very recent work has begun to explore the use of ALD for perovskite solar cells,¹⁵⁰⁻¹⁵³ and we expect that ALD will play a growing role in the understanding and development of interfaces in perovskite absorber based cells. ALD may also find future application in developing inorganic hole conducting materials for solid-state mesoporous sensitized solar cells (in dye, quantum dot and perovskite). The commonly used hole conductors e.g., spiro-OMeTAD do not efficiently fill the mesoporous structures, which prevents the hole-conducting path between the sensitizer and the hole conductor. ALD may be advantageous in filling these mesoporous structures with inorganic hole conductors. As new nanostructured designs for PV continue to be developed, ALD is ready to play a role in modifying interfaces for improved performance due to its ability to deposit conformal coatings of a variety of materials with precise thickness control.

5. Acknowledgments

This work was supported as part of the Center for Nanostructuring for Efficient Energy Conversion (CNEEC), an Energy Frontier Research Center (EFRC) funded by the U.S. Department of Energy, Office of Science, Basic Energy Sciences under Award No. DE-SC0001060 (SFB, PKS) and by The Precourt Institute for Energy (AFP).

6. References

1. *Key World Energy Statistics 2014*, International Energy Agency, 2014.
2. N. S. Lewis and G. Crabtree, *Basic Research Needs for Solar Energy Utilization*, U.S. Department of Energy, 2005.
3. C. Breyer and A. Gerlach, *Prog. Photovolt. Res. Appl.*, 2012, **21**, 121-136.
4. D. Feldman, G. Barbose, R. Margolis, R. Wiser, N. Darghouth and A. Goodrich, *Photovoltaic (PV) Pricing Trends: Historical, Recent, and Near-Term Projections*, Lawrence Berkeley National Laboratory, 2012.
5. K. Ardani, G. Barbose, R. Margolis, R. Wiser, D. Feldman and S. Ong, *Benchmarking Non-Hardware Balance of System (Soft) Costs for U.S. Photovoltaic Systems Using a Data-Driven Analysis from PV Installer Survey Results*, SunShot, U.S. Department of Energy, 2012.
6. M. Green, presented in part at the 2006 IEEE 4th World Conference on Photovoltaic Energy Conference, 2006.
7. G. Conibeer, *Mater. Today*, 2007, **10**, 42-50.
8. M. C. Beard, J. M. Luther, O. E. Semonin and A. J. Nozik, *Acc. Chem.Res.*, 2012, **46**, 1252-1260.
9. G. F. Brown and J. Wu, *Laser & Photon. Rev.*, 2009, **3**, 394-405.
10. G. Conibeer, presented in part at the SPIE Solar Energy + Technology, Aug 20, 2009.
11. J. Hofstetter, J. F. Lelièvre, C. del Cañizo and A. Luque, *Mater. Sci. Eng. B*, 2009, **159-160**, 299-304.
12. S. A. Mann, M. J. de Wild-Scholten, V. M. Fthenakis, W. G. J. H. M. van Sark and W. C. Sinke, *Prog. Photovolt. Res. Appl.*, 2013, **22**, 1180-1194.

13. V. Fthenakis, *Renew. Sust. Energ. Rev.*, 2009, **13**, 2746-2750.
14. G. Goncher and R. Solanki, presented in part at the Proc. SPIE-Int. Soc. Opt. Eng., Aug 28, 2008.
15. K. E. Roelofs, T. P. Brennan and S. F. Bent, *J. Phys. Chem. Lett.*, 2014, **5**, 348-360.
16. H. A. Atwater and A. Polman, *Nature Mater.*, 2010, **9**, 205-213.
17. D. Kuang, S. Ito, B. Wenger, C. Klein, J.-E. Moser, R. Humphry-Baker, S. M. Zakeeruddin and M. Grätzel, *J. Am. Chem. Soc.*, 2006, **128**, 4146-4154.
18. T. Debnath, P. Maity, T. Banerjee, A. Das and H. N. Ghosh, *J. Phys. Chem. C*, 2015, **119**, 3522-3529.
19. M. Grätzel, *J. Photochem. Photobiol. C*, 2003, **4**, 145-153.
20. A. Hagfeldt, G. Boschloo, L. Sun and L. Kloo, *Chem. Rev.*, 2010, **110**, 6595-6663.
21. B. O'Regan and M. Grätzel, *Nature*, 1991, **353**, 737-740.
22. S. Mathew, A. Yella, P. Gao, R. Humphry-Baker, B. F. E. Curchod, N. Ashari-Astani, I. Tavernelli, U. Rothlisberger, M. K. Nazeeruddin and M. Grätzel, *Nature Chem.*, 2014, **6**, 242-247.
23. R. Könenkamp, *Phys. Rev. B.*, 2000, **61**, 11057-11064.
24. S. Yanagida, Y. Yu and K. Manseki, *Acc. Chem. Res.*, 2009, **42**, 1827-1838.
25. C.-Y. Chen, M. Wang, J. Y. Li, N. Pootrakulchote, L. Alibabaei, C. h. Ngoc-le, J. D. Decoppet, J. H. Tsai, C. Grätzel, C. G. Wu, S. M. Zakeeruddin and M. Grätzel, *ACS Nano*, 2009, **3**, 3103-3109.
26. T. Daeneke, T. H. Kwon, A. B. Holmes, N. W. Duffy, U. Bach and L. Spiccia, *Nature Chem.*, 2011, **3**, 213-217.
27. M. Grätzel, U. Bach, D. Lupo, P. Comte, J. E. Moser, F. Weissörtel, J. Salbeck and H. Spreitzer, *Nature*, 1998, **395**, 583-585.
28. K. E. Roelofs, T. P. Brennan, J. C. Dominguez, C. D. Bailie, G. Y. Margulis, E. T. Hoke, M. D. McGehee and S. F. Bent, *J. Phys. Chem. C*, 2013, **117**, 5584-5592.
29. I. Chung, B. Lee, J. He, R. P. H. Chang and M. G. Kanatzidis, *Nature*, 2012, **485**, 486-489.
30. S. Rühle, M. Shalom and A. Zaban, *ChemPhysChem*, 2010, **11**, 2290-2304.
31. O. Niiitsoo, S. K. Sarkar, C. Pejoux, S. Rühle, D. Cahen and G. Hodes, *J. Photochem. Photobiol. A*, 2006, **181**, 306-313.
32. Z. Zheng, L. Zhao, M. Wang, M. Liu, M. S. Marcus and Y. Liu, presented in part at the 2010 35th IEEE Photovoltaic Specialists Conference (PVSC), 2007.
33. C. Lévy-Clément, R. Tena-Zaera, M. A. Ryan, A. Katty and G. Hodes, *Adv. Mater.*, 2005, **17**, 1512-1515.
34. H. J. Lee, M. Wang, P. Chen, D. R. Gamelin, S. M. Zakeeruddin, M. Grätzel and M. K. Nazeeruddin, *Nano Lett.*, 2009, **9**, 4221-4227.
35. N. Guijarro, T. Lana-Villarreal, I. Mora-Seró, J. Bisquert and R. Gómez, *J. Phys. Chem. C*, 2009, **113**, 4208-4214.
36. I. Mora-Seró and J. Bisquert, *J. Phys. Chem. Lett.*, 2010, **1**, 3046-3052.
37. Y. Li, K. Zhao, J. Wang, X. Zhong and J. Bisquert, *J. Am. Chem. Soc.*, 2014, **136**, 9203-9210.

38. A. G. Pattantyus-Abraham, I. J. Kramer, A. R. Barkhouse, X. Wang, G. Konstantatos, R. Debnath, L. Levina, I. Raabe, M. K. Nazeeruddin, M. Grätzel and E. H. Sargent, *ACS Nano*, 2010, **4**, 3374-3380.
39. A. J. Labelle, S. M. Thon, S. Masala, M. M. Adachi, H. Dong, M. Farahani, A. H. Ip, A. Fratalocchi and E. H. Sargent, *Nano Lett.*, 2015, **15**, 1101-1108.
40. B. B. Smith and A. J. Nozik, *Nano Lett.*, 2001, **1**, 36-41.
41. T. Mentzel, V. Porter, S. Geyer, K. MacLean, M. Bawendi and M. Kastner, *Phys. Rev. B*, 2008, **77**, 075316.
42. Y. Liu, M. Gibbs, C. L. Perkins, J. Tolentino, M. H. Zarghami, J. Bustamante, Jorge and M. Law, *Nano Lett.*, 2011, **11**, 5349-5355.
43. D. Zhitomirsky, O. Voznyy, L. Levina, S. Hoogland, K. W. Kemp, A. H. Ip, S. M. Thon and E. H. Sargent, *Nat. Commun.*, 2014, **5**, 1-7.
44. K. S. Leschkies, T. J. Beatty, M. S. Kang, D. J. Norris and E. S. Aydil, *ACS Nano*, 2009, **3**, 3638-3648.
45. T. Suntola and J. Antson, *US Patent Office*, 4058430, 1977.
46. T. Suntola, *Mater. Sci. Rep.*, 1989, **4**, 261-312.
47. S. M. George, *Chem. Rev.*, 2010, **110**, 111-131.
48. C. Hägglund, G. Zeltzer, R. Ruiz, I. Thomann, H. B. R. Lee, M. L. Brongersma and S. F. Bent, *Nano Lett.*, 2013, **13**, 3352-3357.
49. J. R. Bakke, K. L. Pickrahn, T. P. Brennan and S. F. Bent, *Nanoscale*, 2011, **3**, 3482-3508.
50. H. B. Profijt, S. E. Potts, M. C. M. van de Sanden and W. M. M. Kessels, *JVST A*, 2011, **29**, 050801.
51. H. B. R. Lee, S. H. Baeck, T. F. Jaramillo and S. F. Bent, *Nano Lett.*, 2013, **13**, 457-463.
52. J. Heo, S. J. Won, D. Eom, S. Y. Lee, Y. B. Ahn, C. S. Hwang and H. J. Kim, *Electrochem. Solid-State Lett.*, 2008, **11**, 210-213.
53. V. Miikkulainen, M. Leskelä, M. Ritala and R. L. Puurunen, *J. Appl. Phys.*, 2013, **113**, 021301.
54. P. Poodt, D. C. Cameron and E. Dickey, *JVST A*, 2012, **30**, 010802.
55. J. A. van Delft, D. Garcia-Alonso and W. M. M. Kessels, *Semicond. Sci. Technol.*, 2012, **27**, 074002.
56. W. Niu, X. Li, S. K. Karuturi, D. W. Fam, H. Fan, S. Shrestha, L. H. Wong and A. I. Y. Tok, *Nanotechnology*, 2015, **26**, 064001.
57. W. W. Yu, L. H. Qu, W. Z. Guo and X. G. Peng, *Chem. Mater.*, 2003, **15**, 2854-2860.
58. C. B. Murray, D. J. Norris and M. G. Bawendi, *J. Am. Chem. Soc.*, 1993, **115**, 8706-8715.
59. D. D. Sarma, A. Nag, P. K. Santra, A. Kumar, S. Sapra and P. Mahadevan, *J. Phys. Chem. Lett.*, 2010, **1**, 2149-2153.
60. M. Soreni-Harari, N. Yaacobi-Gross, D. Steiner, A. Aharoni, U. Banin, O. Millo and N. Tessler, *Nano Lett.*, 2008, **8**, 678-684.
61. P. K. Santra, A. F. Palmstrom, J. T. Tanskanen, N. Yang and S. F. Bent, *J. Phys. Chem. C*, 2015, **119**, 2996-3005.
62. W. A. Tisdale, K. J. Williams, B. A. Timp, D. J. Norris, E. S. Aydil and X. Y. Zhu, *Science*, 2010, **328**, 1543-1547.

63. R. J. Ellingson, M. C. Beard, J. C. Johnson, P. Yu, O. I. Micic, A. J. Nozik, A. Shabaev and A. L. Efros, *Nano Lett.*, 2005, **5**, 865-871.
64. T. Kannianen, S. Lindroos, J. Ihanus and M. Leskela, *J. Mater. Chem.*, 1996, **6**, 983-986.
65. H. Lee, M. K. Wang, P. Chen, D. R. Gamelin, S. M. Zakeeruddin, M. Grätzel and M. K. Nazeeruddin, *Nano Lett.*, 2009, **9**, 4221-4227.
66. M. Nikumbh, V. Gore and R. B. Gore, *Renew. Energy*, 1997, **11**, 459-467.
67. M. F. Hossain, S. Biswas and T. Takahashi, *Thin Solid Films*, 2009, **518**, 1599-1602.
68. N. Guijarro, T. Lana-Villarreal, I. Mora-Sero, J. Bisquert and R. Gomez, *J. Phys. Chem. C*, 2009, **113**, 4208-4214.
69. P. K. Santra and P. V. Kamat, *J. Am. Chem. Soc.*, 2013, **135**, 877-885.
70. P. K. Santra, P. V. Nair, K. G. Thomas and P. V. Kamat, *J. Phys. Chem. Lett.*, 2013, **4**, 722-729.
71. H. B. R. Lee, M. N. Mullings, X. Jiang, B. M. Clemens and S. F. Bent, *Chem. Mater.*, 2012, **24**, 4051-4059.
72. J. S. King, A. Wittstock, J. Biener, S. O. Kucheyev, Y. M. Wang, T. F. Baumann, S. K. Giri, A. V. Hamza, M. Baeumer and S. F. Bent, *Nano Lett.*, 2008, **8**, 2405-2409.
73. T. P. Brennan, P. Ardalan, H. B. R. Lee, J. R. Bakke, I.-K. Ding, M. D. McGehee and S. F. Bent, *Adv. Energy Mater.*, 2011, **1**, 1169-1175.
74. T. P. Brennan, O. Trejo, K. E. Roelofs, J. Xu, F. B. Prinz and S. F. Bent, *J. Mater. Chem. A*, 2013, **1**, 7566-7571.
75. J. Hao, J. Wang, X. Liu, W. J. Padilla, L. Zhou and M. Qiu, *Appl. Phys. Lett.*, 2010, **96**, 251104.
76. N. Liu, M. Mesch, T. Weiss, M. Hentschel and H. Giessen, *Nano Lett.*, 2010, **10**, 2342-2348.
77. C. Hägglund, G. Zeltzer, R. Ruiz, A. Wangperwang, K. E. Roelofs and S. F. Bent, unpublished work.
78. B. C. O'Regan and F. Lenzmann, *J. Phys. Chem. B*, 2004, **108**, 4342-4350.
79. T. P. Brennan, J. R. Bakke, I.-K. Ding, B. E. Hardin, W. H. Nguyen, R. Mondal, C. D. Bailie, G. Y. Margulis, E. T. Hoke, A. Sellinger, M. D. McGehee and S. F. Bent, *Phys. Chem. Chem. Phys.*, 2012, **14**, 12130-12140.
80. I. K. Ding, N. Tétreault, J. Brillet, B. E. Hardin, E. H. Smith, S. J. Rosenthal, F. Sauvage, M. Grätzel and M. D. McGehee, *Adv. Funct. Mater.*, 2009, **19**, 2431-2436.
81. J. Melas-Kyriazi, I. K. Ding, A. Marchioro, A. Punzi, B. E. Hardin, G. F. Burkhard, N. Tétreault, M. Grätzel, J.-E. Moser and M. D. McGehee, *Adv. Energy Mater.*, 2011, **1**, 407-414.
82. H. J. Snaith and L. Schmidt-Mende, *Adv. Mater.*, 2007, **19**, 3187-3200.
83. J. Krüger, R. Plass, M. Grätzel, P. J. Cameron and L. M. Peter, *J. Phys. Chem. B*, 2003, **107**, 7536-7539.
84. N. Cai, S. J. Moon, L. Cevey-Ha, T. Moehl, R. Humphry-Baker, P. Wang, S. M. Zakeeruddin and M. Grätzel, *Nano Lett.*, 2011, **11**, 1452-1456.
85. B. C. O'Regan, S. Scully, A. C. Mayer, E. Palomares and J. Durrant, *J. Phys. Chem. B*, 2005, **109**, 4616-4623.

86. N. Kopidakis, K. D. Benkstein, J. van de Lagemaat and A. J. Frank, *J. Phys. Chem. B*, 2003, **107**, 11307-11315.
87. E. Palomares, J. N. Clifford, S. A. Haque, T. Lutz and J. R. Durrant, *J. Am. Chem. Soc.*, 2003, **125**, 475-482.
88. C. Lin, F. Y. Tsai, M. H. Lee, C. H. Lee, T. C. Tien, L. P. Wang and S. Y. Tsai, *J. Mater. Chem.*, 2009, **19**, 2999-3003.
89. M. D. Groner, F. H. Fabreguette, J. W. Elam and S. M. George, *Chem. Mater.*, 2004, **16**, 639-645.
90. T. C. Tien, F. M. Pan, L. P. Wang, F. Y. Tsai and C. Lin, *J. Phys. Chem. C*, 2010, **114**, 10048-10053.
91. K. Park, Q. Zhang, B. B. Garcia, X. Zhou, Y.-H. Jeong and G. Cao, *Adv. Mater.*, 2010, **22**, 2329-2332.
92. V. Ganapathy, B. Karunagaran and S.-W. Rhee, *J. Power Sources*, 2010, **195**, 5138-5143.
93. T. C. Li, M. r. S. Góes, F. Fabregat-Santiago, J. Bisquert, P. R. Bueno, C. Prasittichai, J. T. Hupp and T. J. Marks, *J. Phys. Chem. C*, 2009, **113**, 18385-18390.
94. E. Palomares, J. N. Clifford, S. A. Haque, T. Lutz and J. R. Durrant, *Chem. Comm.*, 2002, DOI: 10.1039/b202515a, 1464-1465.
95. D. B. Menzies, Q. Dai, L. Bourgeois and R. A. Caruso, *Nanotechnology*, 2007, **18**, 125608.
96. J. Kim, H. Choi, C. Nahm, C. Kim, S. Nam, S. Kang, D. R. Jung, J. I. Kim, J. Kang and B. Park, *J. Power Sources*, 2012, **220**, 108-113.
97. L. J. Antila, M. J. Heikkilä, V. Mäkinen, N. Humalamäki, M. Laitinen, V. Linko, P. Jalkanen, J. Toppari, V. Aumanen, M. Kemell, P. Myllyperkiö, K. Honkala, H. Häkkinen, M. Leskelä and J. E. I. Korppi-Tommola, *J. Phys. Chem. C*, 2011, **115**, 16720-16729.
98. D. J. Lee, J. Y. Kwon, J. I. Lee and K. B. Kim, *J. Phys. Chem. C*, 2011, **115**, 15384-15389.
99. T. P. Brennan, J. T. Tanskanen, K. E. Roelofs, J. W. F. To, W. H. Nguyen, J. R. Bakke, I. K. Ding, B. E. Hardin, A. Sellinger, M. D. McGehee and S. F. Bent, *J. Phys. Chem. C*, 2013, **117**, 24138-24149.
100. M. Shanmugam, M. F. Baroughi and D. Galipeau, *Thin Solid Films*, 2010, **518**, 2678-2682.
101. T. W. Hamann, O. K. Farha and J. T. Hupp, *J. Phys. Chem. C*, 2008, **112**, 19756-19764.
102. C. Prasittichai and J. T. Hupp, *J. Phys. Chem. Lett.*, 2010, **1**, 1611-1615.
103. M. Law, L. E. Greene, A. Radenovic, T. Kuykendall, a. Jan Liphardt and P. Yang, *J. Phys. Chem. B*, 2006, **110**, 22652-22663.
104. T. C. Tien, F. M. Pan, L. P. Wang, C. H. Lee, Y. L. Tung, S. Y. Tsai, C. Lin, F. Y. Tsai and S. J. Chen, *Nanotechnology*, 2009, **20**, 305201.
105. B. M. Klahr and T. W. Hamann, *J. Phys. Chem. C*, 2009, **113**, 14040-14045.
106. X. Gao, D. Guan, J. Huo, J. Chen and C. Yuan, *Nanoscale*, 2013, **5**, 10438-10446.
107. A. R. Pascoe, L. Bourgeois, N. W. Duffy, W. Xiang and Y. B. Cheng, *J. Phys. Chem. C*, 2013, **117**, 25118-25126.

108. J. Y. Kim, K. H. Lee, J. Shin, S. H. Park, J. S. Kang, K. S. Han, M. M. Sung, N. Pinna and Y. E. Sung, *Nanotechnology*, 2014, **25**, 504003.
109. L. Li, S. Chen, C. Xu, Y. Zhao, N. G. Rudawski and K. J. Ziegler, *ACS Appl. Mater Interfac.*, 2014, **6**, 20978-20984.
110. A. K. Chandiran, M. K. Nazeeruddin and M. Grätzel, *Adv. Funct. Mater.*, 2013, **24**, 1615-1623.
111. N. Tétreault, É. Arsenault, L. P. Heiniger, N. Soheilnia, J. Brillet, T. Moehl, S. Zakeeruddin, G. A. Ozin and M. Grätzel, *Nano Lett.*, 2011, **11**, 4579-4584.
112. A. K. Chandiran, N. Tétreault, R. Humphry-Baker, F. Kessler, E. Baranoff, C. Yi, M. K. Nazeeruddin and M. Grätzel, *Nano Lett.*, 2012, **12**, 3941-3947.
113. R. Ihly, J. Tolentino, Y. Liu, M. Gibbs and M. Law, *ACS Nano*, 2011, **5**, 8175-8186.
114. M. A. van Huis, L. T. Kunneman, K. Overgaag, Q. Xu, G. Pandraud, H. W. Zandbergen and D. Vanmaekelbergh, *Nano Lett.*, 2008, **8**, 3959-3963.
115. P. Schapotschnikow, M. A. van Huis, H. W. Zandbergen, D. Vanmaekelbergh and T. J. H. Vlugt, *Nano Lett.*, 2010, **10**, 3966-3971.
116. A. Pourret, P. Guyot-Sionnest and J. W. Elam, *Adv. Mater.*, 2009, **21**, 232-235.
117. J. Tang, K. W. Kemp, S. Hoogland, K. S. Jeong, H. Liu, L. Levina, M. Furukawa, X. Wang, R. Debnath, D. Cha, K. W. Chou, A. Fischer, A. Amassian, J. B. Asbury and E. H. Sargent, *Nature Mater.*, 2011, **10**, 765-771.
118. P. Nagpal and V. I. Klimov, *Nat. Commun.*, 2011, **2**, 486.
119. J. Tang, L. Brzozowski, D. A. R. Barkhouse, X. Wang, R. Debnath, R. Wolowiec, E. Palmiano, L. Levina, A. G. Pattantyus-Abraham, D. Jamakosmanovic and E. H. Sargent, *ACS Nano*, 2010, **4**, 869-878.
120. Y. Liu, J. Tolentino, M. Gibbs, R. Ihly, C. L. Perkins, Y. Liu, N. Crawford, J. C. Hemminger and M. Law, *Nano Lett.*, 2013, **13**, 1578-1587.
121. H. M. So, H. Choi, H. C. Shim, S. M. Lee, S. Jeong and W. S. Chang, *Appl. Phys. Lett.*, 2015, **106**, 093507.
122. W. Yoon, J. E. Boercker, M. P. Lumb, D. Placencia, E. E. Foos and J. G. Tischler, *Sci. Rep.*, 2013, **3**, 2225.
123. M. G. Panthani, C. J. Stolle and D. K. Reid, *J. Phys. Chem. C*, 2013, **4**, 2030-2034.
124. B. Hoex, S. B. S. Heil, E. Langereis, M. C. M. van de Sanden and W. M. M. Kessels, *Appl. Phys. Lett.*, 2006, **89**, 042112.
125. B. Vermang, V. Fjallstrom, X. Gao and M. Edoff, *IEEE J. Photovolt.*, 2014, **4**, 486-492.
126. Y. Xuan, H. C. Lin, P. D. Ye and G. D. Wilk, *Appl. Phys. Lett.*, 2006, **88**, 263518.
127. Y. Liu, M. Gibbs, J. Puthussery, S. Gaik, R. Ihly, H. W. Hillhouse and M. Law, *Nano Lett.*, 2010, **10**, 1960-1969.
128. B. A. Timp and X. Y. Zhu, *Surf. Sci.*, 2010, **604**, 1335-1341.
129. J. J. Choi, Y.-F. Lim, M. E. B. Santiago-Berrios, M. Oh, B.-R. Hyun, L. Sun, A. C. Bartnik, A. Goedhart, G. G. Malliaras, H. D. Abruña, F. W. Wise and T. Hanrath, *Nano Lett.*, 2009, **9**, 3749-3755.
130. K. S. Leschkies, M. S. Kang, E. S. Aydil and D. J. Norris, *J. Phys. Chem. C*, 2010, **114**, 9988-9996.
131. M. C. Beard, *J. Phys. Chem. Lett.*, 2011, **2**, 1282-1288.
132. J. B. Sambur, T. Novet and B. A. Parkinson, *Science*, 2010, **330**, 63-66.

133. R. Schaller and V. Klimov, *Phys. Rev. Lett.*, 2004, **92**, 186601.
134. J. J. H. Pijpers, R. Ulbricht, K. J. Tielrooij, A. Osherov, Y. Golan, C. Delerue, G. Allan and M. Bonn, *Nat. Phys.*, 2009, **5**, 811-814.
135. P. Tyagi and P. Kambhampati, *J. Chem. Phys.*, 2011, **134**, 094706.
136. G. Nair, L. Y. Chang, S. M. Geyer and M. G. Bawendi, *Nano Lett.*, 2011, **11**, 2145-2151.
137. A. J. Nozik, *Chem. Phys. Lett.*, 2008, **457**, 3-11.
138. S. ten Cate, Y. Liu, C. S. Suchand Sandeep, S. Kinge, A. J. Houtepen, T. J. Savenije, J. M. Schins, M. Law and L. D. A. Siebbeles, *J. Phys. Chem. Lett.*, 2013, **4**, 1766-1770.
139. R. W. Zehner, B. F. Parsons, R. P. Hsung and L. R. Sita, *Langmuir*, 1999, **15**, 1121-1127.
140. A. Vilan, A. Shanzer and D. Cahen, *Nature*, 2000, **404**, 166-168.
141. Y. Liu, S. R. Scully, M. D. McGehee, J. Liu, C. K. Luscombe, J. M. J. Fréchet, S. E. Shaheen and D. S. Ginley, *J. Phys. Chem. B*, 2006, **110**, 3257-3261.
142. S. Yang, D. Prendergast and J. B. Neaton, *Nano Lett.*, 2012, **12**, 383-388.
143. C. H. M. Chuang, P. R. Brown, V. Bulović and M. G. Bawendi, *Nature Mater.*, 2014, **13**, 796-801.
144. C. A. Wilson, R. K. Grubbs and S. M. George, *Chem. Mater.*, 2005, **17**, 5625-5634.
145. A. N. Goldstein, C. M. Echer and A. P. Alivisatos, *Science*, 1992, **256**, 1425-1427.
146. D. H. Levy, D. Freeman, S. F. Nelson, P. J. Cowdery-Corvan and L. M. Irving, *Appl. Phys. Lett.*, 2008, **92**, 192101.
147. N. P. Dasgupta, X. Meng, J. W. Elam and A. B. F. Martinson, *Acc. Chem. Res.*, 2015, **48**, 341-348.
148. R. W. Johnson, A. Hultqvist and S. F. Bent, *Mater. Today*, 2014, **17**, 236-246.
149. M. A. Green, K. Emery, Y. Hishikawa, W. Warta and E. D. Dunlop, *Prog. Photovolt. Res. Appl.*, 2014, **23**, 1-9.
150. H. Wei, J. Shi, X. Xu, J. Xiao, J. Luo, J. Dong, S. Lv, L. Zhu, H. Wu, D. Li, Y. Luo, Q. Meng and Q. Chen, *Phys. Chem. Chem. Phys.*, 2015, **17**, 4937-4944.
151. X. Dong, X. Fang, M. Lv, B. Lin, S. Zhang, J. Ding and N. Yuan, *J. Mater. Chem. A*, 2015, **3**, 5360-5367.
152. B. R. Sutherland, S. Hoogland, M. M. Adachi, P. Kanjanaboos, C. T. O. Wong, J. J. McDowell, J. Xu, O. Voznyy, Z. Ning, A. J. Houtepen and E. H. Sargent, *Adv. Mater.*, 2014, **27**, 53-58.
153. X. Dong, H. Hu, B. Lin, J. Ding and N. Yuan, *Chem. Comm.*, 2014, **50**, 14405-14408.